# Hydrodynamic Forces on Inundated Bridge Decks

PUBLICATION NO. FHWA-HRT-09-028

MAY 2009

U.S. Department of Transportation
**Federal Highway Administration**

Research, Development, and Technology
Turner-Fairbank Highway Research Center
6300 Georgetown Pike
McLean, VA 22101-2296

## FOREWORD

The Hydrodynamic Forces on Inundated Bridge Decks Study described in this report was conducted at the Federal Highway Administration's (FHWA) Turner-Fairbank Highway Research Center (TFHRC) J. Sterling Jones Hydraulics Laboratory and at the Department of Energy's Argonne National Laboratory's (Argonne) Transportation Research and Analysis Computing Center (TRACC). The study was in response to a request of several State transportation departments asking for new design guidance to predict hydrodynamic forces on bridge decks for riverine conditions. The study included experiments (physical modeling) at the TFHRC J. Sterling Jones Hydraulics Laboratory and High Performance Computational Fluid Dynamics (CFD) modeling at the Argonne National Laboratory. This report will be of interest to hydraulic engineers and bridge engineers who are involved in estimating loads for bridge decks. This report is being distributed as an electronic document through the TFHRC Web site (www.tfhrc.gov).

Cheryl Allen Richter
Acting Director, Office of Infrastructure
Research and Development



## Quality Assurance Statement

The Federal Highway Administration (FHWA) provides high-quality information to serve Government, industry, and the public in a manner that promotes public understanding. Standards and policies are used to ensure and maximize the quality, objectivity, utility, and integrity of its information. FHWA periodically reviews quality issues and adjusts its programs and processes to ensure continuous quality improvement.

# TECHNICAL REPORT DOCUMENTATION PAGE

| 1. Report No.<br>FHWA-HRT-09-028 | 2. Government Accession No. | 3. Recipient's Catalog No.<br>N/A |
|---|---|---|
| 4. Title and Subtitle<br>Hydrodynamic Forces on Inundated Bridge Decks | | 5. Report Date<br>May 2009 |
| | | 6. Performing Organization Code<br>N/A |
| 7. Author(s)<br>Kornel Kerenyi, Tanju Sofu, and Junke Guo | | 8. Performing Organization Report No. |
| 9. Performing Organization Name and Address<br>GKY and Associates, Inc.<br>4229 Lafayette Center Dr., Suite 1850<br>Chantilly, VA 20151<br>University of Nebraska<br>312 N. 14th Street<br>Alexander Building West<br>Lincoln, NE 68588-0430 | | 10. Work Unit No. (TRAIS)<br>N/A |
| | | 11. Contract or Grant No.<br>DTFH-04-C-00037 |
| 12. Sponsoring Agency Name and Address<br>Office of Infrastructure Research and Development<br>Federal Highway Administration<br>6300 Georgetown Pike<br>McLean, VA 22101-2296 | | 13. Type of Report and Period Covered<br>Laboratory Report<br>November 2005–June 2008 |
| | | 14. Sponsoring Agency Code<br>FHWA Task Order 16 |

15. Supplementary Notes
Contracting Officer's Technical Representative (COTR): Kornel Kerenyi, HRDI-07
Lars Hanson summarized the results and described the procedures used in this study. Afzal Bushra, Zhaoding Xie, and Oscar Berrios provided invaluable assistance with instrumentation, data collection, and analysis.

16. Abstract

The hydrodynamic forces experienced by an inundated bridge deck have great importance in the design of bridges. Specifically, the drag force, lift force, and the moment acting on the bridge deck under various levels of inundation and a range of flow conditions influence the design and construction of the bridge. This report explores the forces acting on bridges in two ways. First, through physical experimentation on scaled-down bridge deck models tested in a flume and then with computational fluid dynamics (CFD) simulation models. Three bridge deck prototypes were used for the experimentation: a typical six-girder highway bridge deck, a three-girder deck, and a streamlined deck designed to better withstand the hydraulic forces. The forces (expressed as nondimensional force coefficients) on each of the bridge deck shapes were measured in the laboratory with an ultra-precise force balance under a range of inundation scenarios (including partial inundation) and at four different velocities characterized by Froude numbers in the range of 0.16 to 0.32.

CFD modeling was performed using both the Fluent® and STAR-CD® software packages. The CFD models were calibrated to the flow conditions of the six-girder bridge, and these same conditions were used for the other two bridge shapes. A range of model options were tested including two-dimensional versus three-dimensional models, different mesh resolutions, boundary conditions, and turbulence models; their effect on the accuracy of results and processing efficiency were noted.

Fitting equations were generated to create an envelope around the experimental data and create design charts for each of the bridge types and force coefficients.

Finally, the CFD models, though they can match some of the general behavior of experimental models in terms of the relationship between inundation ratio and force measured at the bridge, do not yet faithfully reproduce the critical values of the hydraulic forces and show very little response to velocity. The CFD simulations seem promising as a method to test bridge designs, but more research is needed before complex designs can be tested wholly in the CFD realm. However, the design charts from the experimental results should be a valuable tool for the bridge designer in a wide range of design applications.

| 17. Key Words<br>Hydrodynamic Forces, Force Balance, CFD, Inundated bridge decks | 18. Distribution Statement<br>No restrictions. This document is available to the public through the National Technical Information Service (NTIS), Springfield, VA 22161. | | |
|---|---|---|---|
| 19. Security Classif. (of this report)<br>Unclassified | 20. Security Classif. (of this page)<br>Unclassified | 21. No. of Pages<br>44 | 22. Price |

Form DOT F 1700.7 (8-72) Reproduction of completed page authorized.

# SI* (MODERN METRIC) CONVERSION FACTORS

## APPROXIMATE CONVERSIONS TO SI UNITS

| Symbol | When You Know | Multiply By | To Find | Symbol |
|---|---|---|---|---|
| | | **LENGTH** | | |
| in | inches | 25.4 | millimeters | mm |
| ft | feet | 0.305 | meters | m |
| yd | yards | 0.914 | meters | m |
| mi | miles | 1.61 | kilometers | km |
| | | **AREA** | | |
| $in^2$ | square inches | 645.2 | square millimeters | $mm^2$ |
| $ft^2$ | square feet | 0.093 | square meters | $m^2$ |
| $yd^2$ | square yard | 0.836 | square meters | $m^2$ |
| ac | acres | 0.405 | hectares | ha |
| $mi^2$ | square miles | 2.59 | square kilometers | $km^2$ |
| | | **VOLUME** | | |
| fl oz | fluid ounces | 29.57 | milliliters | mL |
| gal | gallons | 3.785 | liters | L |
| $ft^3$ | cubic feet | 0.028 | cubic meters | $m^3$ |
| $yd^3$ | cubic yards | 0.765 | cubic meters | $m^3$ |
| | NOTE: volumes greater than 1000 L shall be shown in $m^3$ | | | |
| | | **MASS** | | |
| oz | ounces | 28.35 | grams | g |
| lb | pounds | 0.454 | kilograms | kg |
| T | short tons (2000 lb) | 0.907 | megagrams (or "metric ton") | Mg (or "t") |
| | | **TEMPERATURE (exact degrees)** | | |
| °F | Fahrenheit | 5 (F-32)/9<br>or (F-32)/1.8 | Celsius | °C |
| | | **ILLUMINATION** | | |
| fc | foot-candles | 10.76 | lux | lx |
| fl | foot-Lamberts | 3.426 | $candela/m^2$ | $cd/m^2$ |
| | | **FORCE and PRESSURE or STRESS** | | |
| lbf | poundforce | 4.45 | newtons | N |
| $lbf/in^2$ | poundforce per square inch | 6.89 | kilopascals | kPa |

## APPROXIMATE CONVERSIONS FROM SI UNITS

| Symbol | When You Know | Multiply By | To Find | Symbol |
|---|---|---|---|---|
| | | **LENGTH** | | |
| mm | millimeters | 0.039 | inches | in |
| m | meters | 3.28 | feet | ft |
| m | meters | 1.09 | yards | yd |
| km | kilometers | 0.621 | miles | mi |
| | | **AREA** | | |
| $mm^2$ | square millimeters | 0.0016 | square inches | $in^2$ |
| $m^2$ | square meters | 10.764 | square feet | $ft^2$ |
| $m^2$ | square meters | 1.195 | square yards | $yd^2$ |
| ha | hectares | 2.47 | acres | ac |
| $km^2$ | square kilometers | 0.386 | square miles | $mi^2$ |
| | | **VOLUME** | | |
| mL | milliliters | 0.034 | fluid ounces | fl oz |
| L | liters | 0.264 | gallons | gal |
| $m^3$ | cubic meters | 35.314 | cubic feet | $ft^3$ |
| $m^3$ | cubic meters | 1.307 | cubic yards | $yd^3$ |
| | | **MASS** | | |
| g | grams | 0.035 | ounces | oz |
| kg | kilograms | 2.202 | pounds | lb |
| Mg (or "t") | megagrams (or "metric ton") | 1.103 | short tons (2000 lb) | T |
| | | **TEMPERATURE (exact degrees)** | | |
| °C | Celsius | 1.8C+32 | Fahrenheit | °F |
| | | **ILLUMINATION** | | |
| lx | lux | 0.0929 | foot-candles | fc |
| $cd/m^2$ | $candela/m^2$ | 0.2919 | foot-Lamberts | fl |
| | | **FORCE and PRESSURE or STRESS** | | |
| N | newtons | 0.225 | poundforce | lbf |
| kPa | kilopascals | 0.145 | poundforce per square inch | $lbf/in^2$ |

*SI is the symbol for the International System of Units. Appropriate rounding should be made to comply with Section 4 of ASTM E380.
(Revised March 2003)

## TABLE OF CONTENTS


**1. INTRODUCTION ..... 1**

**2. THEORY AND APPROACH ..... 3**
- **THEORY OF FORCES ACTING ON INUNDATED BRIDGE DECKS ..... 3**
- **HYDRAULIC FORCE MEASUREMENT EXPERIMENTAL SETUP ..... 5**
- **PIV SETUP ..... 8**
- **COMPUTING AND TRACC ..... 9**

**3. COMPUTATIONAL FLUID DYNAMICS SETUP AND VALIDATION ..... 11**
- **STAR-CD® ..... 11**
  - Numerical Configuration ..... 11
- **FLUENT® ..... 15**
  - Numerical Configuration ..... 15
- **SIMULATION SUMMARY ..... 17**

**4. RESULTS ..... 19**
- **COMPARISON OF SIMULATED (FLUENT®) RESULTS WITH PIV EXPERIMENTAL DATA ..... 19**
- **RESULTS FOR THE SIX-GIRDER BRIDGE DECK ..... 22**
- **RESULTS FOR THE THREE-GIRDER BRIDGE DECK ..... 25**
- **RESULTS FOR THE STREAMLINED DECK ..... 28**
- **FITTING EQUATIONS AND COEFFICIENT VALUES ..... 31**

**5. DECK FORCE CALCULATION EXAMPLES ..... 33**

**6. CONCLUSION ..... 37**

## LIST OF FIGURES

Figure 1. Diagram. Scaled six-girder bridge deck model used in assessments of drag and lift forces and the nomenclature for bridge deck and flume dimensions ..... 3
Figure 2. Equation. Inundation ratio ..... 4
Figure 3. Equation. Froude number ..... 4
Figure 4. Diagram. Definition sketch of forces acting on bridge deck ..... 4
Figure 5. Equation. Drag coefficient ..... 4
Figure 6. Equation. Lift coefficient ..... 5
Figure 7. Equation. Moment coefficient ..... 5
Figure 8. Diagram. Dimensions of the six-girder bridge deck ..... 6
Figure 9. Diagram. Dimensions of the three-girder bridge deck ..... 6
Figure 10. Diagram. Dimensions of the streamlined bridge deck ..... 6
Figure 11. Diagram. Side view of railings with dimensions for the six-girder and three-girder bridge decks ..... 6
Figure 12. Diagram. Test section of deck force analyzer showing strain gauge configuration ..... 7
Figure 13. Photo. Deck force analyzer system at the TFHRC hydraulics lab ..... 8
Figure 14. Image. Comparison of flow fields for the 2-D and 3-D models for the STAR-CD® simulations ..... 12
Figure 15. Image. Segment of bridge used for 3-D model ..... 13
Figure 16. Diagram. Coarse meshes for STAR-CD® simulation ..... 14
Figure 17. Diagram. Partially refined meshes for STAR-CD® simulation ..... 14
Figure 18. Model. A rendering of the 3-D six-girder bridge deck in Fluent® ..... 16
Figure 19. Image. Velocity profile from the 2-D Fluent® model ..... 16
Figure 20. Image. Velocity profile from the 3-D Fluent® model ..... 17
Figure 21. Diagram. Fluent® unstructured mesh in the vicinity of the bridge ..... 17
Figure 22. Image. Velocity profile from the Fluent® k-ε CFD model for the six-girder bridge ..... 20
Figure 23. Image. PIV velocity profile for the six-girder bridge ..... 20
Figure 24. Image. Velocity profile from the Fluent® k-ε CFD model for the three-girder bridge ..... 21
Figure 25. Image. PIV velocity profile for the three-girder bridge ..... 21
Figure 26. Image. Velocity profile from the Fluent® k-ε CFD model for the streamlined bridge ..... 22
Figure 27. Image. PIV velocity profile for the streamlined bridge ..... 22
Figure 28. Graph. Drag coefficient versus inundation ratio for the six-girder bridge ..... 23
Figure 29. Graph. Lift coefficient versus inundation ratio for the six-girder bridge ..... 24
Figure 30. Graph. Moment coefficient versus inundation ratio for the six-girder bridge ..... 25
Figure 31. Graph. Drag coefficient versus inundation ratio for the three-girder bridge ..... 26
Figure 32. Graph. Lift coefficient versus inundation ratio for the three-girder bridge ..... 27
Figure 33. Graph. Moment coefficient versus inundation ratio for three-girder bridge ..... 28
Figure 34. Graph. Drag coefficient versus inundation ratio for streamlined bridge deck ..... 29
Figure 35. Graph. Lift coefficient versus inundation ratio for the streamlined bridge ..... 30
Figure 36. Graph. Moment coefficient versus inundation ratio for the streamlined bridge ..... 30
Figure 37. Equation. Drag coefficient fitting equation for three- and six-girder bridges ..... 31
Figure 38. Equation. Lift coefficient fitting equation for three- and six-girder bridges ..... 31
Figure 39. Equation. Moment coefficient fitting equation for all bridge types ..... 31

Figure 40. Equation. Drag coefficient fitting equation for the streamlined bridge..... 31
Figure 41. Equation. Lift coefficient fitting equation for the streamlined bridge..... 31
Figure 42. Equation. Upper fitting equation for drag coefficient as a function of $h^*$ ..... 34
Figure 43. Equation. Total drag force per unit length on the example six-girder bridge for the 1,000-year flood..... 34
Figure 44. Equation. Velocity, $v$, at $h^*_{crit}$ ..... 35

## LIST OF TABLES

Table 1. Fitting equation coefficient values for six-girder (6-g) and three-girder (3-g) bridges.. 32
Table 2. Fitting equation coefficient values for the streamlined bridge ..... 32
Table 3. Critical coefficient values by bridge type ..... 32
Table 4. Bridge example dimensions..... 33
Table 5. Flow conditions for example design floods..... 33
Table 6. High and low force coefficients for the two example floods..... 34

## LIST OF ACRONYMS AND ABBREVIATIONS

| | |
|---|---|
| 2-D | Two-dimensional |
| 3-D | Three-dimensional |
| ADV | Acoustic Doppler Velocimeter |
| Argonne | Department of Energy's Argonne National Laboratory |
| CFD | Computational fluid dynamics |
| FHWA | Federal Highway Administration |
| LES | Large Eddy Simulation |
| PISO | Pressure-Implicit Split-Operator |
| PIV | Particle Image Velocimetry |
| PVC | Polyvinyl Chloride |
| R&D | Research and development |
| RANS | Reynolds-averaged Navier-Stokes |
| SIMPLE | Semi-Implicit Method for Pressure Linked Equations |
| TFHRC | Turner-Fairbank Highway Research Center |
| TRACC | Transportation Research and Analysis Computing Center |
| VoF | Volume of fluid |

## LIST OF SYMBOLS

| | |
|---|---|
| $C_D$ | Drag coefficient |
| $C_L$ | Lift coefficient |
| $C_M$ | Moment coefficient |
| $F_D$ | Drag force |
| $F_L$ | Lift force |
| Fr | Froude number |
| g | Gravitational acceleration |
| h* | Inundation ratio |
| $h^*_{crit}$ | Critical Inundation ratio resulting in maximum forces |
| $h_b$ | Height from bottom of flume to bottom of bridge |
| $h_u$ | Height of water from bottom of flume |
| k-ε | Turbulence model |
| L | Bridge length |
| $M_{cg}$ | Moment about the center of gravity |
| Re | Reynolds number |
| s | Deck thickness |
| V, v | Free stream velocity |
| W | Bridge width |
| ρ | Fluid density (or water density) |

# 1. INTRODUCTION

When a bridge crossing a waterway is partially or entirely submerged during a flood event, its deck may be subjected to significant hydrodynamic loading. The proper estimation of loading exerted by the flow on the structure is important for design and evaluation of vulnerability. This report uses a combination of reduced scale experiments and computer modeling to investigate the forces on inundated bridges.

The analysts at Argonne National Laboratory (Argonne), a U.S. Department of Energy laboratory, are working in collaboration with the researchers at the Federal Highway Administration's (FHWA) Turner-Fairbank Highway Research Center (TFHRC) to study computational fluid dynamics (CFD) techniques for simulating open channel flow around inundated bridges. The reduced scale experiments conducted at the TFHRC J. Sterling Jones Hydraulics Laboratory established the foundation of validated computational models of the same phenomena. The overall objectives of the study for which this report is based was to investigate the forces on inundated bridges and to establish validated computational practices to address the research needs of the transportation community in bridge hydraulics.

Bridges are a critical component of the nation's transportation network. Evaluation of a bridge's stability during and after flooding events, including the structural response of the bridge, is critical to highway safety. During a flood or tsunami, highway bridges over large waterways may become partially or completely submerged. Flood flows add significant hydrodynamic loading on bridges, resulting in possible shearing or overturning of the bridge deck and failure of the bridge superstructures. Traditionally, bridge analysts and designers have relied on expensive scaled experiments to provide estimates of the flow field and structural response. With the rapid development of supercomputing technology, commercial CFD code provides a quick, economic way to study these systems. The availability of parallel computers and analysis capabilities of commercially available software provides an opportunity to shift these evaluations into the CFD domain. When validated using the broad experimental database, the use of CFD simulations will allow expanded parametric analysis and provide a means of directly evaluating the effects of scaling.

The general external flow characteristics of a submerged body depend on the shape of the body. Generally, streamlined bodies (i.e., airfoils, streamlined cars) have little influence on the fluid around them compared with the effect from blunt bodies (i.e., triangle shapes and square-bodied bridge decks). The drag and lift on a bridge deck depend on many variables, notably the height of the free-surface level in relation to the bridge deck and the Reynolds number (*Re*) or Froude number (*Fr*), both of which describe the amount of turbulence in the flow and the degree to which the flow is critical. There are different mechanisms that have to be considered between the partially inundated case and completely inundated case. For a partially inundated deck, accurate estimates of hydrodynamic loading must take into account not only the forces from the upstream flow field but also the influence of free surface due to the hydrodynamic force from waves. For the completely inundated deck neglecting the effect of wave forces, the mean flow field upstream dominates the hydrodynamic loading on the bridge deck.

For a body moving through a fluid or a body immersed in a moving fluid, the interaction between the body and the fluid surrounding it produces forces at the fluid-body interface. The forces acting parallel to the free-stream direction due to the influence of viscosity may be called *wall shear stresses,* and the force acting normal to the free-stream direction due to pressure may be called *normal stresses.* The resultant force of shear stress and pressure distribution in the velocity's direction is termed as *drag,* and the resultant force normal to the direction of velocity is termed *lift.*

As flow separates from the leading edge corner for a bridge deck, large numbers of vortices form at different scales along the surface of the bridge deck. Eventually, they shed from the trailing edge in a process called the *vortex shedding phenomenon.* The center of a vortex, or a vortex core, has a local minimum pressure. Thus, the formation and development of the vortices tend to dominate the progression of the drag, lift, and moment on the surface of the bridge deck. Different deck geometries submerged by the flow have different flow fields and distributions of vortices along the surface of the decks leading to the alterations of forces or the force coefficients with the change in the geometry.

The applicability of commercial CFD software to predict flow field and evaluate drag and lift forces is being investigated. CFD provides a prediction of fluid flow by means of numerical modeling and software tools. It enables scientists and engineers to perform experiments (i.e., computer simulations) in virtual flow laboratory and significantly reduces the amount of experimentation and overall cost. CFD is a highly interdisciplinary research area that lies at the interface of physics, applied mathematics, and computer science.

The CFD-based simulations can be used for a range of hydraulics research, including the assessment of lift and drag forces on flooded bridge decks, shape optimizations to minimize pressure scour and pier erosion, analysis of sediment transport and its influence on scour, evaluation of active or passive countermeasures for damage mitigation, and consideration of environmental issues such as fish passage through culverts. Currently, the applicability of the commercial CFD software for prediction of these phenomena is being investigated, and the agreement between the code predictions and experimental data from TFHRC flumes is presented in this report.

## 2. THEORY AND APPROACH

The study for this report investigated the forces acting on inundated bridge decks through physical experimental testing and CFD modeling with two commercial software packages. Three types of bridges were tested for their reaction to drag forces, lift forces, and moment-generating forces in relation to the degree of inundation (inundation ratio). The bridge types included traditional six-girder and three-girder shapes, and prototype streamlined deck shapes designed to reduce the force load during inundation.

The first technical task performed for this study was the analysis of drag and lift forces and moments for inundated bridge decks as a function of immersion height and flow rate. The analysis results for these prototypical open channel flow configurations were compared to the force balance and Particle Image Velocimetry (PIV) measurements from TFHRC tests to validate the corresponding CFD models. Both two-dimensional (2-D) and three-dimensional (3-D) models of the bridge decks with six- and three-girders were studied using Fluent® and STAR-CD® CFD software. A set of simulations were completed to assess the impact of various modeling options, including the following, while always considering accuracy of results and computational efficiency:

- The influence of the free surface.
- The effects of channel wall.
- Mesh sensitivity study for grid independent solutions.
- Turbulence model evaluations.

### THEORY OF FORCES ACTING ON INUNDATED BRIDGE DECKS

In determining the structural response of the bridge decks, both the properties of the fluid and the configuration of the bridge were important. Consistent with the experimental methodology, the nomenclature for bridge and flume dimensions are illustrated in figure 1.

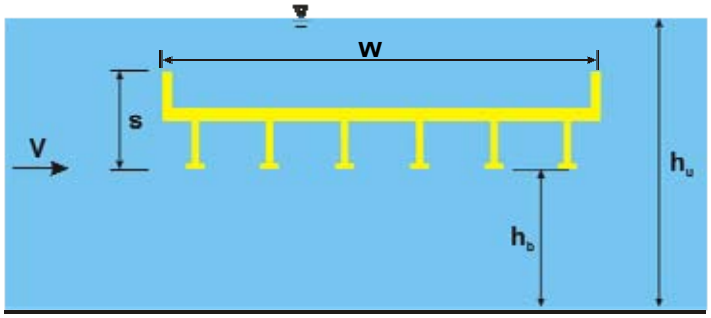


**Figure 1. Diagram. Scaled six-girder bridge deck model used in assessments of drag and lift forces and the nomenclature for bridge deck and flume dimensions.**

In determining the forces on bridges, the properties of the flowing stream that had the greatest impact were the height of the water and its velocity. The height of the water surface in relation to the flume dimension, the position of the bridge deck, as well as the flow velocity can be

expressed as the inundation ratio, $h^*$. Shown in figure 2, the inundation ratio is a measure of the difference between the height of the free surface over the low chord of the bridge deck ($h_u - h_b$) divided by the deck thickness, $s$. Higher values of $h^*$ mean that the bridge is more submerged. The flow velocity can be characterized by the dimensionless *Fr*. *Fr* (figure 3) is expressed as the free stream velocity, $v$, over the square root of the depth of flow multiplied by the gravitational acceleration, $g$

$$h^* = \frac{h_u - h_b}{s}$$

**Figure 2. Equation. Inundation ratio.**

$$Fr = \frac{v}{\sqrt{gh_u}}$$

**Figure 3. Equation. Froude number.**

There were three primary responses of the bridge deck to the flowing water. Figure 4 illustrates the forces acting on a submerged bridge deck. The drag force, $F_D$, acting parallel to flow, affects the bridge deck horizontal stability and tends to "push" the bridge off its piers and abutments. The lift force, $F_L$, acts vertically and perpendicular to flow and can lift the bridge deck off of its piers and abutments. Unevenly distributed forces on the bridge decks lead to moments about the center of gravity, $M_{cg}$, of the bridge deck, which can cause the bridge to overturn.

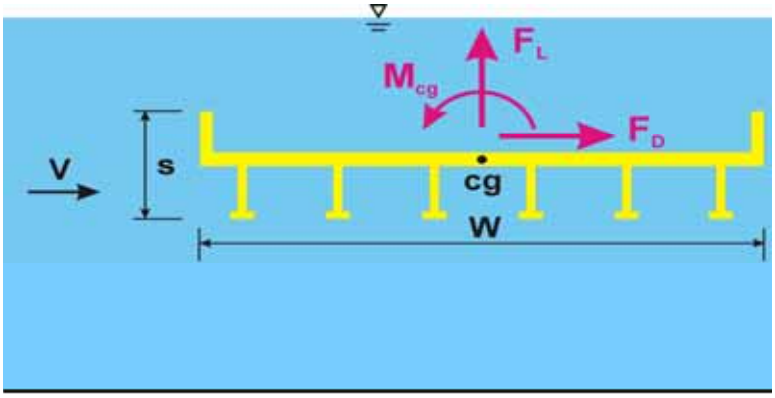


**Figure 4. Diagram. Definition sketch of forces acting on bridge deck.**

The forces of drag and lift and moments acting on the bridge deck are usually expressed in nondimensional coefficient forms. The definition of the coefficient of drag, $C_D$, depends on $h^*$ and is shown in figure 5. The two cases correspond to a partially inundated bridge ($h^* < 1$) and a fully submerged bridge ($h^* > 1$).

$$C_D = \frac{F_D}{\frac{1}{2}\rho v^2 (Ls)}, \text{ if } h^* \geq 1; \text{ and } \quad C_D = \frac{F_D}{\frac{1}{2}\rho v^2 [L(h_u - h_b)]}, \text{ if } h^* < 1$$

**Figure 5. Equation. Drag coefficient.**

The lift coefficient is defined in figure 6. The moment coefficient with respect to the center of gravity of the bridge deck is defined in figure 7.

$$C_L = \frac{F_L}{\frac{1}{2}\rho v^2 (LW)}$$

**Figure 6. Equation. Lift coefficient.**

$$C_M = \frac{M_{cg}}{\frac{1}{2}\rho v^2 (LW^2)}$$

**Figure 7. Equation. Moment coefficient.**

Here, $F_D$ and $F_L$ are the forces integrated over the surface of the bridge deck along the flow and perpendicular directions, respectively, where ρ is the density of water, and $L$ is the length of the bridge (orthogonal to the plane of figure 1). When calculating the integrated vertical force, $F_L$, its component associated with buoyancy force is excluded to be consistent with the experiments in which force balances were calibrated for zero lift under no-flow conditions.

## HYDRAULIC FORCE MEASUREMENT EXPERIMENTAL SETUP

The physical experimental setup was designed to empirically determine the effect of the inundation ratio on the lift, drag, and moment forces for three different bridge prototypes.

The experiments were conducted in a 12.8 m long by 0.4 m wide by 0.5 m high Plexiglas® rectangular flume. The flume was set horizontally, and the depth of flow was controlled with an automatic, adjustable tailgate located at the downstream end of the flume. Flow was supplied by a 0.054-$m^3$/s pumping system. The mean free-surface level was measured using ultrasonic sensors at two cross sections along the flume. An electromagnetic flow meter measured the discharge. An Acoustic Doppler Velocimeter (ADV) probe was used to measure the velocity distribution of the flow.

The following three models of bridge decks were tested in the experiments:

- Six-girder bridge deck (shown in figure 8).
- Three-girder bridge deck (shown in figure 9).
- Streamlined bridge deck (shown in figure 10).

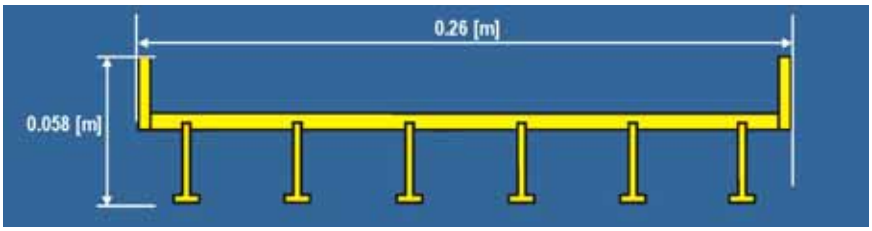


**Figure 8. Diagram. Dimensions of the six-girder bridge deck.**

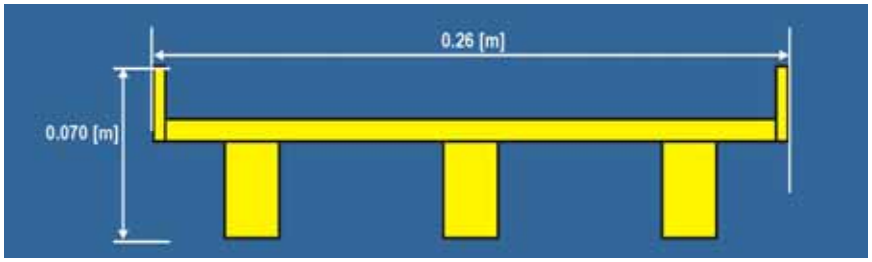


**Figure 9. Diagram. Dimensions of the three-girder bridge deck.**

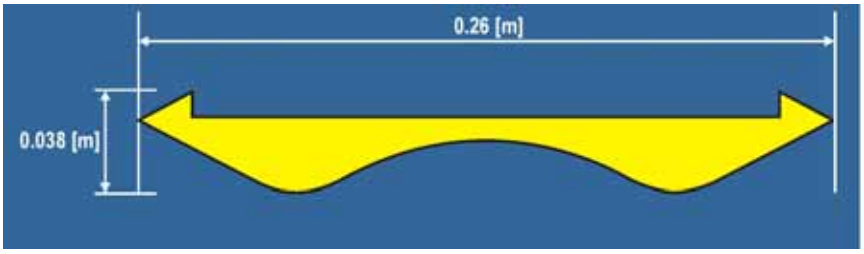


**Figure 10. Diagram. Dimensions of the streamlined bridge deck.**

Both the six-girder and three-girder bridge decks had railings on both sides with the dimensions shown in figure 11.

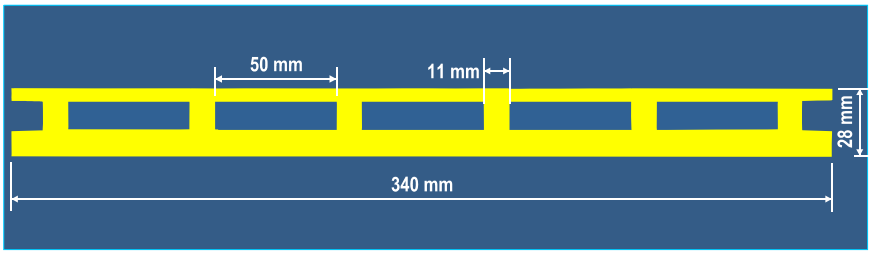


**Figure 11. Diagram. Side view of railings with dimensions for the six-girder and three-girder bridge decks.**

The six-girder bridge, representing a typical U.S. highway bridge deck shape, was constructed out of Polyvinyl Chloride (PVC) at a 1:40 geometrical reduction scale based on the depths, maximum discharges, and inundations possible in the flume. This scaled bridge deck was optimally sized to investigate a range of force values in flow conditions ranging from low to high flows, all at subcritical *Fr* in the upstream flow. The six-girder and three-girder bridge decks had the same width, but the three-girder deck had a 22 percent larger frontal area ($s$ = 0.70 m).

The three bridges were evaluated in the same flume and under the same experimental conditions in order to reduce the experimental error. The experiments were conducted for four approach velocities ranging from 0.25 to 0.5 m/s. The flow depths, $h_u$, in the experiments were always kept at 0.25 m. Under these conditions, the *Fr* varied within the range of 0.16 to 0.32 in response to the changing velocities. The submergence of the bridge deck within the 0.25-m flow depth was varied from slight submergence of the deck girders to complete overtopping of the bridge deck, corresponding to an inundation ratio of $h^* = 0.29$ to roughly 5.0 (for the streamlined bridge).

The measurement of forces on the bridge deck was performed by a deck force analyzer system, which was constructed for this study (figure 12 and figure 13). This transducer system was designed to measure forces induced by the bridge deck model simultaneously in the x-direction (Drag) and z-direction (Lift) by use of electric strain gauges. The bridge deck model was mounted on a bracket and positioned in the flume. The bracket was attached at the platform of the system by four ball-beared pendulums which were connected with the platform by four flat springs. This allowed it to move back and forth in the direction of flow as well as vertically. Motion in each direction was resisted by two pairs of flat springs. The tension in these springs was detected by strain gauges, which generated an electrical signal proportional to the forces upon the bridge deck model in the x-direction (Drag) and z-direction (Lift).

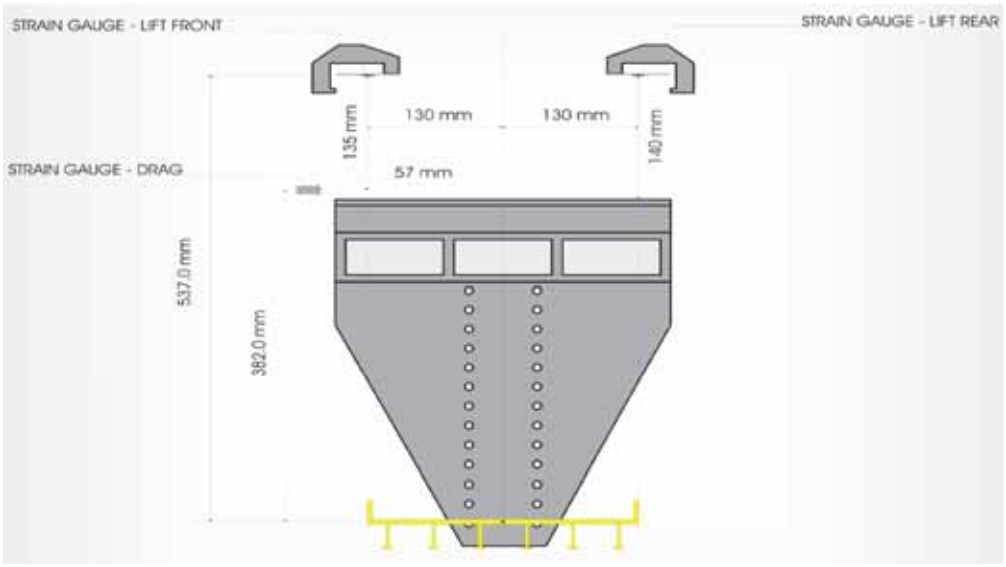


**Figure 12. Diagram. Test section of deck force analyzer showing strain gauge configuration.**

**Figure 13. Photo. Deck force analyzer system at the TFHRC hydraulics lab.**

The transducer was dead-load calibrated prior to use and was checked periodically during data collection. The calibration was performed by running an experiment with still water for each inundation ratio $h^*$. The output of the acquisition data was set as the zero-reference value. The mean drag and lift forces of an experimental run were evaluated by subtracting the corresponding zero-reference value.

## PIV SETUP

A secondary experimental setup was built to examine the flow field around the bridges in detail using PIV, which is a noninvasive measurement technique to visualize flow distributions. The technique involves adding microscopically small particles that are highly reflective to the flow and then using a laser to illuminate a thin layer of the flow so that only the particles in that light sheet reflected the laser's light. Using cameras pointed with different angles toward the light sheet, researchers can capture images of the moving particles. In order to measure the velocity, at least two exposures were needed. They could be recorded on one or several frames. The frames were split in a large number of interrogation areas, or tiles. It was then possible to calculate a displacement vector for each tile with the help of signal processing (an auto correlation/cross correlation algorithm). This was converted to a velocity using the time between image exposures.

The PIV experiment was conducted in a smaller flume with bridge models scaled down by a factor of 1.5. The experiments were conducted for $V$ = 250 mm/s with $h_b$ = 50 mm, 101 mm, and 116 mm and the depth of the flow, $h_u$, as 170 mm.

## COMPUTING AND TRACC

Besides establishing credible experimental data on the response of bridge decks to various forces, a major objective of this study was to establish validated computational practices to address the transportation community's research needs in bridge hydraulics. Traditionally, bridge hydraulics work relies on scaled experiments to provide measurements for flow field, which is the velocity and turbulence of a fluid as functions of position and time. Now, however, parallel computers and commercially available software provide an opportunity to shift the focus of these evaluations to the CFD domain. After being validated using the data from a limited set of experiments, high-fidelity CFD simulations can be used to expand the range and scope of parametric studies. The CFD simulations may be used in the future to predict the effects of scaling by studying differences between the reduced-scale experiments and full-scale bridges.

In this study, the reduced-scale experiments conducted at the TFHRC hydraulics laboratory established the foundations of a CFD-based simulation methodology. Researchers at Argonne and TFHRC worked together to study CFD techniques for simulating open channel flow around inundated bridges. The computationally intensive CFD modeling programs require enormous computing power.

Argonne is leading the initiative to establish the high-performance computing center, Transportation Research and Analysis Computing Center (TRACC), to pursue research and development (R&D) programs. TRACC is a general purpose advanced computing and visualization facility available to the transportation community for a broad spectrum of applications. The TRACC components include high-performance computing, visualization, and networking systems.

Argonne analysts provided technical support to researchers at TFHRC on CFD simulations for this study. Two CFD software packages were investigated for their utility in modeling open channel flow around bridges for this study. The STAR-CD® and Fluent® programs were used in this study to build models of the six- and three-girder bridges and to run simulations. The models were calibrated using the results of the six-girder reduced scale experiments and PIV results. The three-girder bridge deck was simulated using the same calibration settings as the six-girder models to serve as a "blind-test" of validity. The following chapter describes the two models and their numerical configuration and evaluation for this study.

# 3. COMPUTATIONAL FLUID DYNAMICS SETUP AND VALIDATION

Two commercial CFD programs were configured to model the forces on the bridge decks in simulations: STAR-CD® and Fluent®. Building the CFD model involved selecting the mesh resolution, simulation algorithm, boundary conditions including the air-water interface properties, and turbulence model. Additionally, the model simulations investigated the effect of *Fr* and inundation ratio on the three bridge decks in the same manner as the experimental tests.

In addition to testing the ability of the models to replicate the experimental model results, the CFD simulation had a secondary objective to determine the robustness and efficiency of the models. Due in part to scheduling constraints, the CFD model was only calibrated using the six-girder bridge deck experimental results. The same flow configurations were applied to the models of the three-girder and streamlined bridge decks. By comparing these "blind" simulation results with the experimental results, an effective test of the CFD models' general applicability was created. The CFD simulations were also conducted with attention to the efficiency of computation. Even with the TRACC facility, the high computational intensity of CFD modeling demands an efficient model setup to ensure a manageable runtime.

The setup and chosen configuration of the two models are described below.

## STAR-CD®

Cd-adapco's STAR-CD® was used by researchers at the University of Nebraska at Omaha to simulate the forces acting on the three bridge decks. Like many commercial CFD models, STAR-CD® computes the overall flow of the fluid and associated forces by breaking the modeling environment into a mesh of many tiny cells. Then, the enormously complex problems of continuity and energy can be solved at the individual cell level. This project's STAR-CD® approach was based primarily on the structured hexahedral mesh option for modeling.

The STAR-CD®'s solver choices include well established pressure-based solution algorithms like the Pressure-Implicit Split-Operator (PISO) and the Semi-Implicit Method for Pressure Linked Equations (SIMPLE). Although PISO is a more robust scheme with predictor/corrector steps, the alternative SIMPLE scheme can also predict accurate results for approximately half the computational cost. Therefore, the SIMPLE solver was used for the bridge deck simulations.

### Numerical Configuration

To set up the numerical configuration of the simulation, the bridge dimensions and the flow conditions had to be specified.

Since water flows perpendicular to a bridge and the modeled bridge decks had regular cross sections along their length, several simplifications of the CFD model were possible and were used to test for their effectiveness in matching the experimental results and reducing computational time.

Instead of modeling the whole bridge deck at the exact dimensions of the experimental setup, the CFD model could be constructed with just a small portion of the bridge deck. The simplest

model would be a true 2-D model with the bridge modeled in cross section with the thickness of only a single computational cell. To assess the validity of this approach, the 2-D model's flow field was compared to the flow field of a 3-D model that replicated the experimental setup. Instead of a full 3-D model, a half model of the bridge deck with one side along a flume wall and what was once the middle of the bridge along a symmetry boundary was used. The flow field results for the 3-D model along this symmetry plane and the 2-D model are displayed in figure 14. The flow fields indicate sufficient agreement that a 2-D model could be sufficient for the computation of the forces and moments.

The single-cell 2-D model shown in figure 14 does not provide a perfect representation of the six- and three-girder bridge due to the patterns of posts supporting the railings and voids. To account for these differences, an extended 2-D model was created so that one edge of the deck was at the midpoint of a post, and the other edge was at the midpoint of one of the void spaces. This situation is indicated by the yellow stripe in figure 15. By placing symmetry boundaries on both edges, a quasi-infinite bridge deck was simulated. The railings were simulated, as in the physical experiments, on both the leading and trailing edge of the bridge deck.

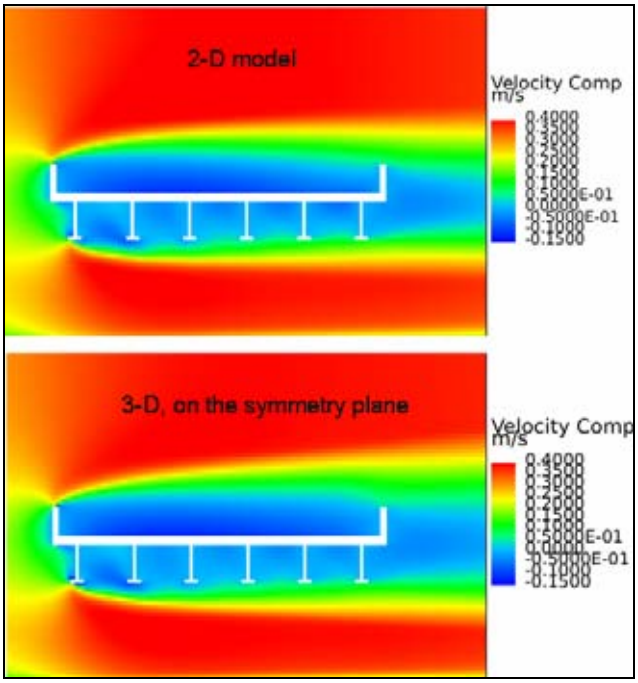


**Figure 14. Image. Comparison of flow fields for the 2-D and 3-D models for the STAR-CD® simulations.**

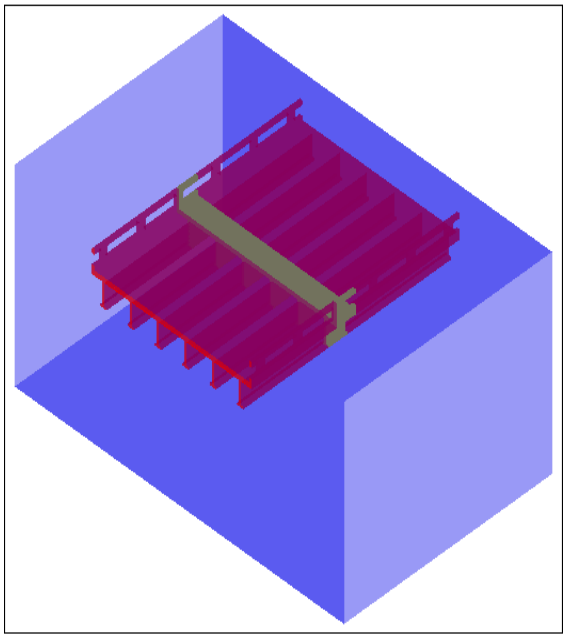

**Figure 15. Image. Segment of bridge used for 3-D model.**

In addition to the bridge model specification, the general simulation mesh had to be specified. Increasing the mesh resolution increased computational time, so the mesh size had to be chosen carefully. Two mesh sizes were simulated. The “coarse grid,” shown in figure 16 and figure 17, had a cell size of 3.5 mm by 2.5 mm by 2.5 mm. The “partially refined” mesh increased the mesh resolution near the bridge by dividing each coarse cell into eight smaller cells by halving the cell along each dimension.

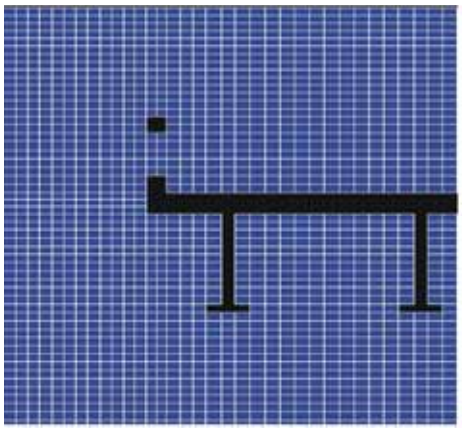

**Figure 16. Diagram. Coarse meshes for STAR-CD® simulation.**

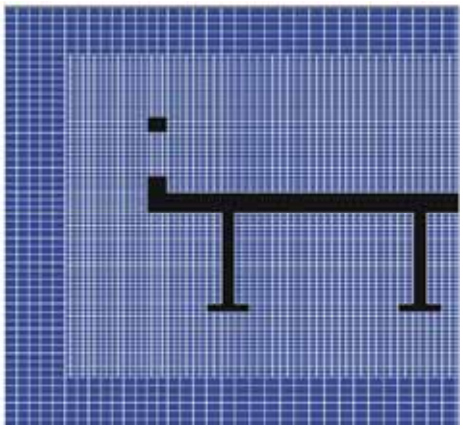

**Figure 17. Diagram. Partially refined meshes for STAR-CD® simulation.**

The parameters of the fluid itself made up the final component of the simulation. The most important considerations were in the treatment of air-water interface and in the turbulence model selected. Advances in computational fluid mechanics have provided the basis for insight into the dynamics of multiphase flows. Since the free surface in open channel flow could be an important feature of the flow field influencing the parameters of interest defined above, the Volume of Fluid (VoF) computational technique was pursued to capture its form accurately. The VoF solution methodology was well suited for free-surface flow problems where the two fluids were separated by a well defined, sharp interface.

The VoF methodology deals with a single continuum whose properties vary according to its composition as derived from solution of transport equations for the component fluids. These component fluids are assumed to be immiscible and labeled as the base, light fluid, (in this study, air) and the heavy fluid (water). The density of each fluid component is assumed constant, and, when both components are present in a computational cell, they share the field variables (velocity and pressure) computed for the fluid mixture. The result is that water depth can vary slightly along the flow path, as it would in reality.

Since the form of the free surface was generally stable and reasonably flat in this study, especially for high inundation ratios ($h^* > 1$), a separate set of calculations in which the top

surface is at $h = h_u$, was modeled as a flat "fixed surface" in STAR-CD®. In these single-phase (water-only) simulations, the top surface was modeled either as a slip-wall or free-stream boundary. As expected, the results of these steady-state "fixed-surface" simulations were generally consistent with the results of the "free-surface" simulations. Since the calculations with the fixed-surface models did not require a long computation time, many of the turbulence model evaluations and grid sensitivity studies were performed with the fixed-surface models in STAR-CD®.

These turbulence models were the final major consideration in the modeling setup. Undoubtedly, the high *Re* flows approaching the bridge decks could be considered turbulent. Turbulent flow is highly unsteady and irregular. The available computer power was not sufficient to represent all of the eddies ranging from the smallest scale (corresponding to dissipative motions) to the largest scale (responsible for most of the momentum transport in a high speed flow). Therefore, turbulence models were used to describe turbulence based on some simplifying assumptions. STAR-CD® provides a range of turbulence modeling options, including several based on the two equation Reynolds-averaged Navier-Stokes (RANS) model and even higher order models. Ultimately, the high *Re* variant of the k-ε model was selected for the detailed simulations.

## FLUENT®

ANSYS, Inc.'s ® Fluent® CFD modeling software was also used for modeling the deck forces on the bridge decks. Though Fluent® and STAR-CD® have many similar capabilities, they were used differently for this study. The following section describes the numerical configuration for Fluent®.

### Numerical Configuration

Though there are many mesh options, the Fluent® experiments for this study used an unstructured mesh as opposed to the structured hexahedral mesh in STAR-CD®. The unstructured mesh captures the flow around complex shapes like the bridge decks. The Tet/Hybrid mesh was chosen, which is composed primarily of tetrahedrons. Figure 18 shows a 3-D model of the six-girder bridge rendered in this mesh.

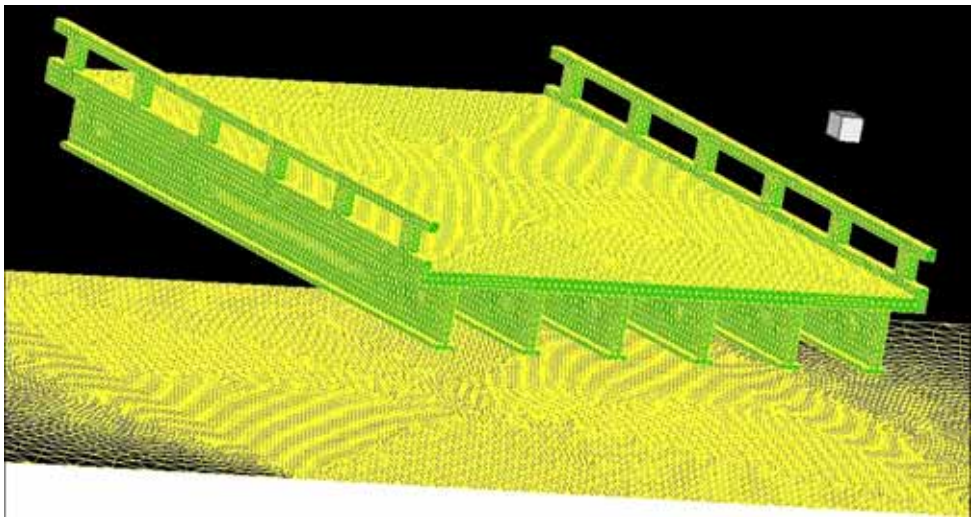

**Figure 18. Model. A rendering of the 3-D six-girder bridge deck in Fluent®.**

The simulations using Fluent® were performed for three different shapes of bridge deck (i.e., six- and three-girder bridge deck models with railings on both sides and streamlined bridge deck). As in the STAR-CD® simulations, 2-D and 3-D models were built and tested for the six-girder bridge deck. The 2-D model was simplified to have a solid wall instead of a railing, but the 3-D model was modeled exactly as in the experiments. The velocity maps in figure 19 and figure 20 show that there was general agreement between the 2-D and 3-D models but that the 3-D model captured more detail and was less affected by the railings.

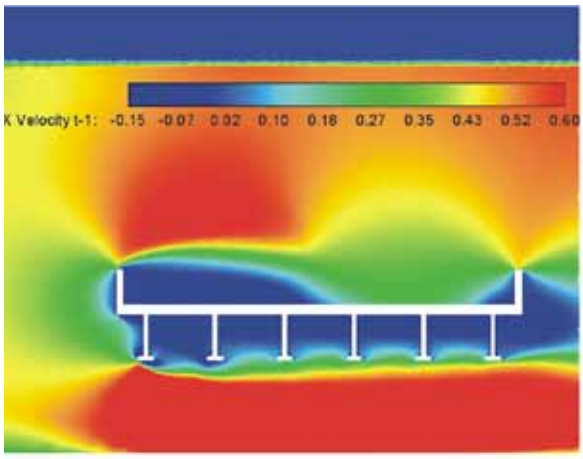


**Figure 19. Image. Velocity profile from the 2-D Fluent® model.**

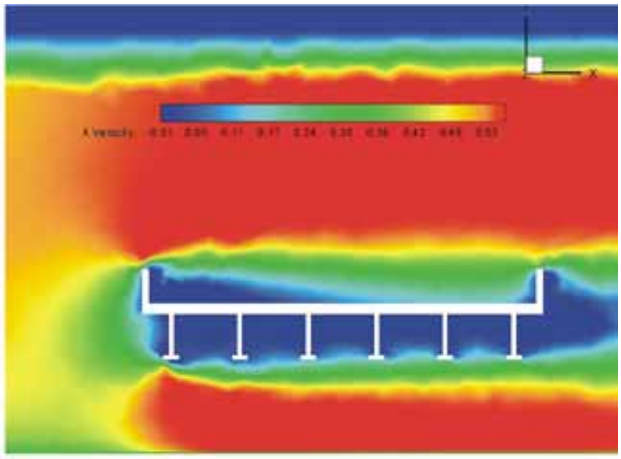

**Figure 20. Image. Velocity profile from the 3-D Fluent® model.**

The simulation mesh was also unstructured and Tet/Hybrid. All simulations were performed with a mesh that was finer in the vicinity of the bridge and coarser farther away, as shown in figure 21. All of the simulations were also performed using the VoF transient multiphase model with both air and water. Since the free surface was an important feature of open channel flow, all of the Fluent® simulations were run for the two-phase model with air and water.

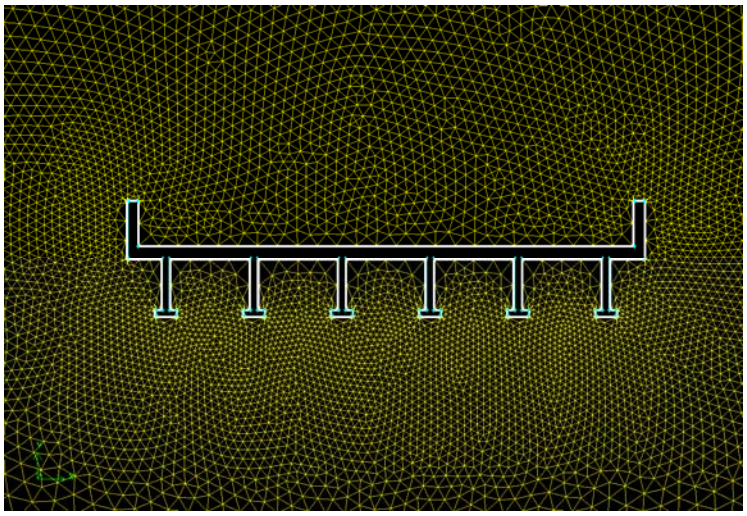

**Figure 21. Diagram. Fluent® unstructured mesh in the vicinity of the bridge.**

The Fluent® software also required selection of a turbulence model to complete the simulation. Two different turbulence models were used in parallel for the Fluent® simulations. The unsteady k-ε model was selected since it was also used in the STAR-CD® simulations. Additionally, the Large Eddy Simulation (LES) model was selected since it simulates large eddy motion explicitly based on flow direction and does not perform time-averaging as the RANS models do. The LES could more faithfully resolve the turbulent flow in the model but at greater computational cost.

## SIMULATION SUMMARY

The first objective of the simulations was to provide estimates of the drag, lift, and moment coefficients using the same variables as in the physical experiment. That is, the simulations were

conducted for approach velocities ranging from 0.25 to 0.5 m/s (*Fr* varied within the range of 0.16 to 0.32), and the simulations were run for various inundation ratios.

The STAR-CD® simulations modeled only the six- and three-girder bridge decks, while the Fluent® k-ε simulations modeled all three types. The Fluent® LES simulation considered only the six-girder deck. The experimental data for six-girder bridge deck model were only available during the numerical simulations, whereas the three-girder and streamlined bridge deck experimental data were provided once the simulations were completed.

# 4. RESULTS

Through both physical experiments and CFD simulation, the forces exerted on the three bridge deck types were analyzed in detail. Before analyzing the performance of the CFD models in estimating the force values, it was important to verify qualitatively that the flow fields generated in the CFD models matched those produced in the PIV experiments. The first section of this chapter describes these comparisons.

The following sections display the results of the experimentation and the CFD simulation on design charts showing the relationship between the inundation ratio ($h^*$) and the unitless coefficients for drag, lift, or moments. The experimental results represent averages of three to five trials performed for each $Fr$ at each inundation ratio. To further expand results, the data were used to calculate parameters for fitting equations which roughly bound the high- and low-force coefficients values. These equations are shown in the drag, lift, and moment plots as blue lines and are also referred to as envelope curves since they generally form and envelope around the experimental results. The form and coefficient values of these equations are laid out in the final section of this chapter.

## COMPARISON OF SIMULATED (FLUENT®) RESULTS WITH PIV EXPERIMENTAL DATA

Figure 22 through figure 27 show comparisons of the simulated velocity contours around the bridge deck to the PIV measurements from the experiments for each bridge type.

The PIV measurements were conducted with smaller scale bridge decks, which were smaller by the factor of 1.5 from the bridge deck used in the evaluations of hydrodynamic forces. The flow conditions compared were for $V$ = 250 mm/s with $h_u$ = 50 mm, 101 mm, and 116 mm and the depth of the flow, $h_u$, as 170 mm. Each PIV image was matched with a velocity map from the CFD model simulated with a similar value of $h^*$. The velocity profiles show the velocity of the water in the direction of flow across the bridge cross section. Red indicates high velocity, while orange, yellow, green, and blue represent progressively slower velocities. Darker blue areas indicate where the flow was not moving or moving in reverse during the experiment, possibly indicating the presence of a stable vortex. The flow field vectors were drawn in both maps, but the PIV vectors were not connected into streamlines as the CFD results were.

In general, the velocity profiles show strong agreement between the flow fields. The three bridge types show noticeable differences. The three-girder bridge easily produced the most substantial vortex zones, with a particularly strong one just downstream of the third-girder bridge. Additionally, the three-girder bridge had a larger zone of no-flow than the six-girder bridge just downstream of the first girder. The six-girder bridge appeared to create a larger disturbance on the top of the bridge, however. Both of these phenomena were most easily seen in the PIV profiles.

The streamlined bridge deck had a much smaller impact on the velocities than the other two deck shapes. As flow encountered the first lobe, there was evidence of contraction-induced acceleration as the velocity above and below increased slightly. The CFD and PIV results for the streamlined bridge differed somewhat in the location of the primary flow obstructions. The CFD

results place two small but noticeable vortices (shown in figure 26) on the downstream edge of both short triangular guardrails. There was virtually no reduction in flow velocity beneath the bridge. The PIV results, however, display a significant zone of very slow flow in the cavity on the underside of the streamlined deck (shown in figure 27).

Overall, the velocities in the flow field seemed quite comparable between the CFD models and PIV experiments. Even minute differences in the flow fields or non-visible flow parameters, however, could lead to significant differences in the simulated force values. The next sections highlight the deck force results.

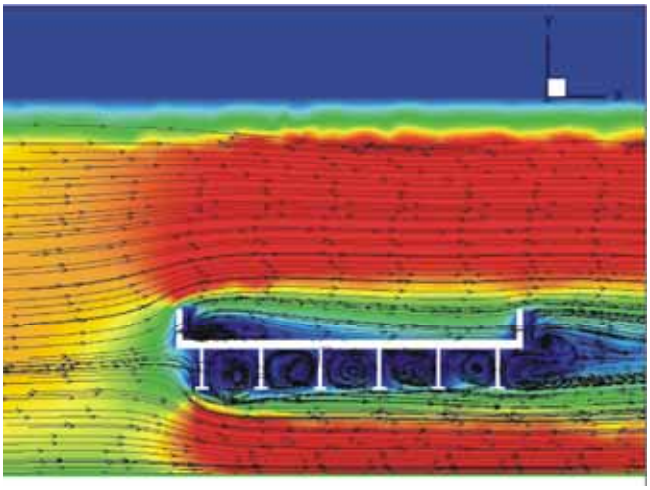

**Figure 22. Image. Velocity profile from the Fluent® k-ε CFD model for the six-girder bridge.**

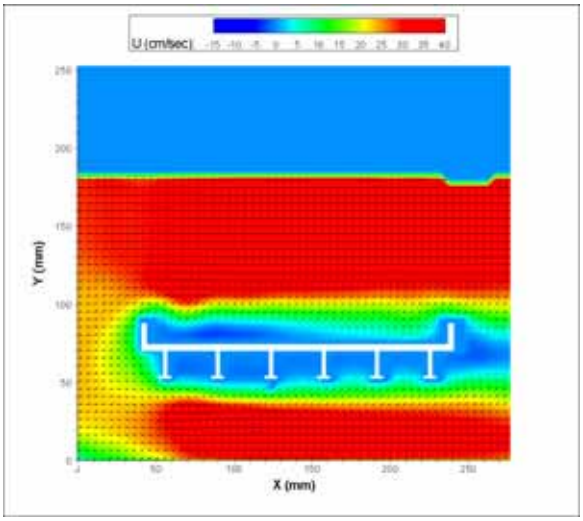


**Figure 23. Image. PIV velocity profile for the six-girder bridge.**

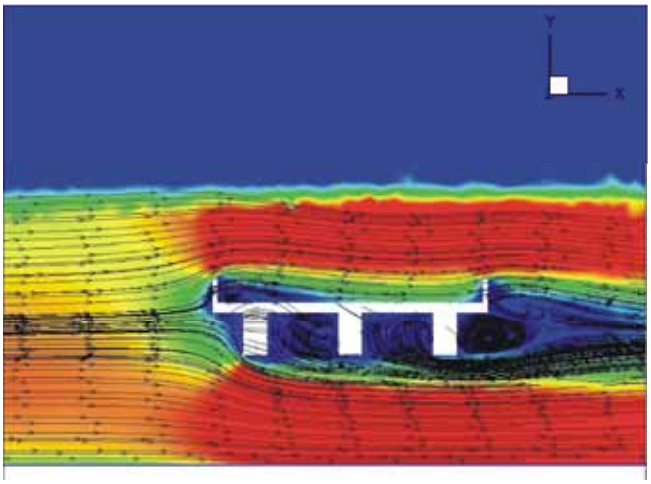

**Figure 24. Image. Velocity profile from the Fluent® k-ε CFD model for the three-girder bridge.**

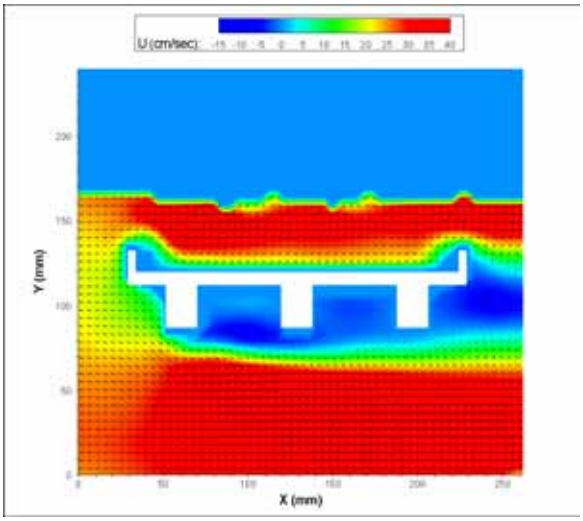


**Figure 25. Image. PIV velocity profile for the three-girder bridge.**

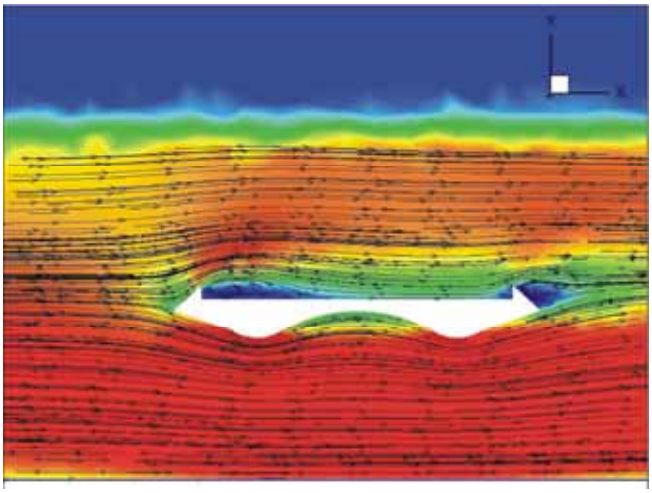

**Figure 26. Image. Velocity profile from the Fluent® k-ε CFD model for the streamlined bridge.**

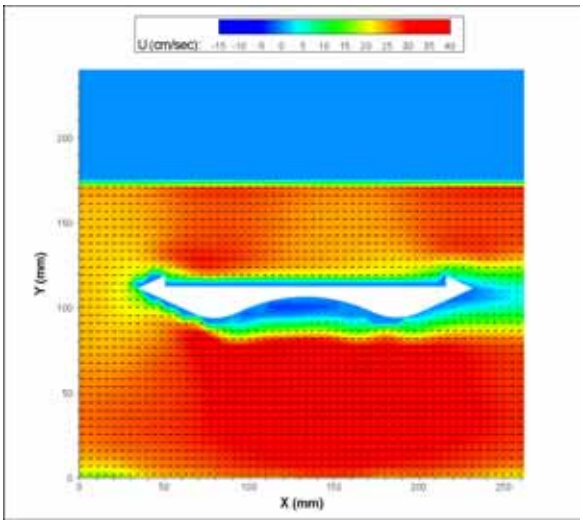


**Figure 27. Image. PIV velocity profile for the streamlined bridge.**

## RESULTS FOR THE SIX-GIRDER BRIDGE DECK

The six-girder bridge deck represented the dimensions of a typical highway bridge deck. The 1:40 scale of the model allowed the range of *Fr* used in the experimentation to correspond well with realistic *Fr* for actual flood flows interacting with bridges.

Figure 28 depicts the relationship of the inundation ratio with the drag coefficient, $C_D$, for the six-girder bridge. The experimental data are shown in four series of points. The fitting equations are shown as lines, and the calibrated results of the STAR-CD® simulation and two Fluent® models are presented as points.

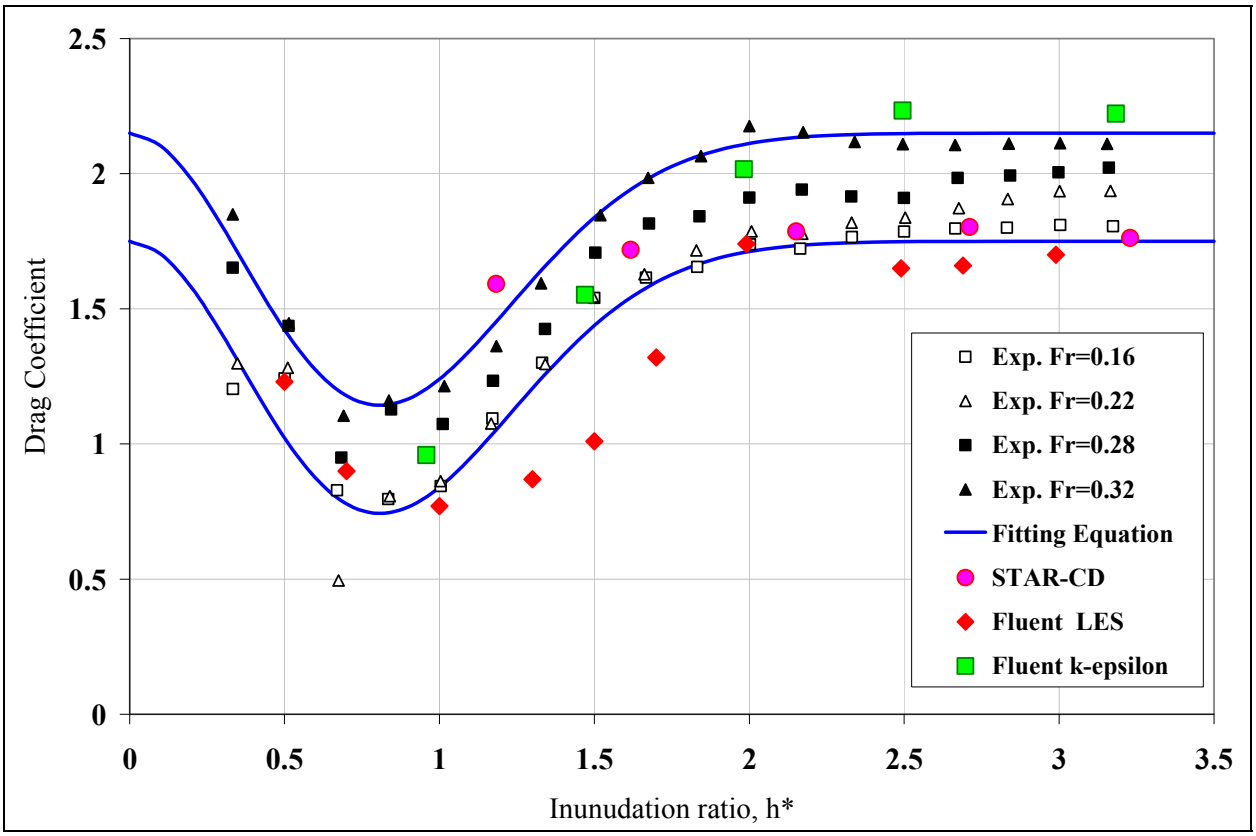


**Figure 28. Graph. Drag coefficient versus inundation ratio for the six-girder bridge.**

The drag coefficient plot shows that the drag coefficient was positive at all values of $h^*$ but that there was a major dip in the drag coefficient at $h^*$ around 0.5–0.8. This corresponds to a case when the bridge was slightly more than halfway inundated, perhaps as the water level was reaching the top of the girders and was beginning to transition to overtopping the deck. As the bridge became more inundated ($h^* > 1.5$), the drag coefficient values leveled off to around 2.

The fitting equations enclose the experimental data generally well over the whole range of inundation ratios.

The CFD models did not show any dependence on *Fr,* so agreement with experimental data should not be overstated. The Fluent® k-ε results showed very good agreement with the experimental data, replicating both the shape and magnitude, but slightly overestimating the maximum values. The Fluent® LES results generally provided low estimates of $C_D$ and did not increase quickly enough in the 1.0 to 2.0 range of $h^*$. The STAR-CD® results showed good agreement at high inundation ratios but did not match the shape of the experimental data below $h^* = 2$.

Figure 29 displays the lift coefficient plot for the six-girder bridge. Experimental data, fitting equations, and CFD simulation results are displayed in the same manner as in the drag coefficient plot. The experimental results revealed that the lift coefficient was negative for all the cases tested. A negative lift coefficient means that the flow was actually exerting a pull-down force on the bridge. While the effect was quite small when the water level was just barely

reaching the bottom of the girders, the lift coefficient rapidly became more negative until *h** roughly equaled 0.65. The lift coefficient slowly returned to 0 as the inundation ratio exceeded 3. As shown in figure 29, the fitting equations are generally representative of the experimental data but break down at higher inundation ratios and higher *Fr*.

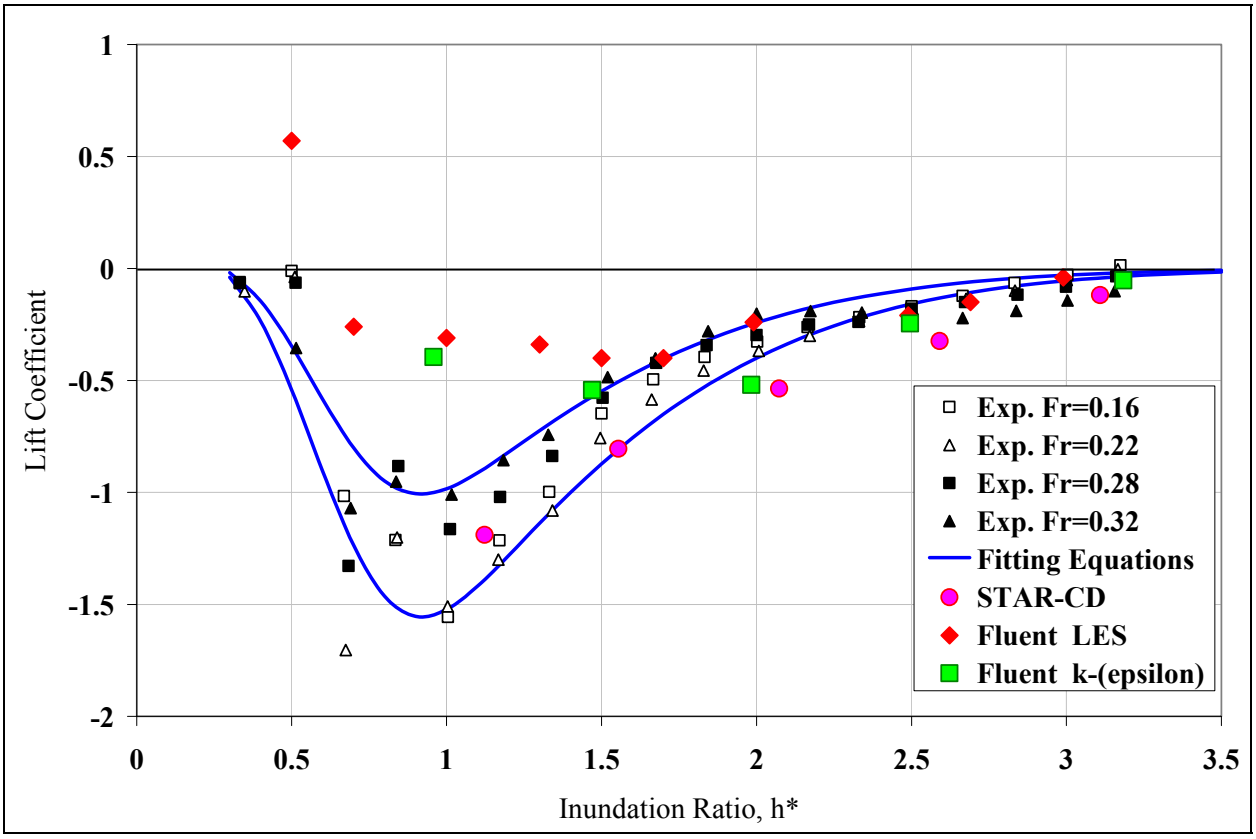


**Figure 29. Graph. Lift coefficient versus inundation ratio for the six-girder bridge.**

The CFD model results did not closely follow the experimental results. The STAR-CD® results roughly captured the gradual increase in lift coefficient but fell below the bottom envelope curve. The two Fluent® models showed major departures from the experimental results' behavior and showed comparatively little influence from the inundation ratio. As shown in the figure, the Fluent® LES results are mostly flat when the experimental results show a considerable drop near $h^* = 1$. Meanwhile, the Fluent® k-ε start above the upper envelope curve but then roughly follow the experimental results at higher values *of h**.

The moment coefficient plot is shown in figure 30. The experimental results demonstrate a similar shape no matter the *Fr* but are intriguing for their relative positions on the moment coefficient axis. There is little difference between the $Fr = 0.16$ and $Fr = 0.22$ cases, and both stay almost completely above 0. This corresponds to a moment rotating the bridge counterclockwise (rotating the upstream side of the bridge down and the downstream side up). The peak moment coefficient came during the study when the bridge was roughly halfway inundated, and the flow was pushing almost entirely on the first girder and thus below the center of gravity. At higher *Fr*, the effect was less pronounced. Additionally, in the 1.5–2 range for *h**,

the moment coefficient became negative and then stabilized for the *Fr* = 0.28 and *Fr* = 0.32 cases, which meant the bridge would turn over in the clockwise direction.

As shown in the figure, the CFD results demonstrate only fair agreement with the experimental results for the moment coefficient. Interestingly, the STAR-CD® and Fluent® k-ε models show moderate agreement with each other. They also show reasonable agreement with some of the experimental results at high inundation ratios, but the moment coefficients are near 0 anyway. The Fluent® LES model has results consistently lower than the experimental *Fr* = 0.16 case. The model represents the reduction in the moment coefficient and stabilization but somewhat more aggressively than in the experimental results.

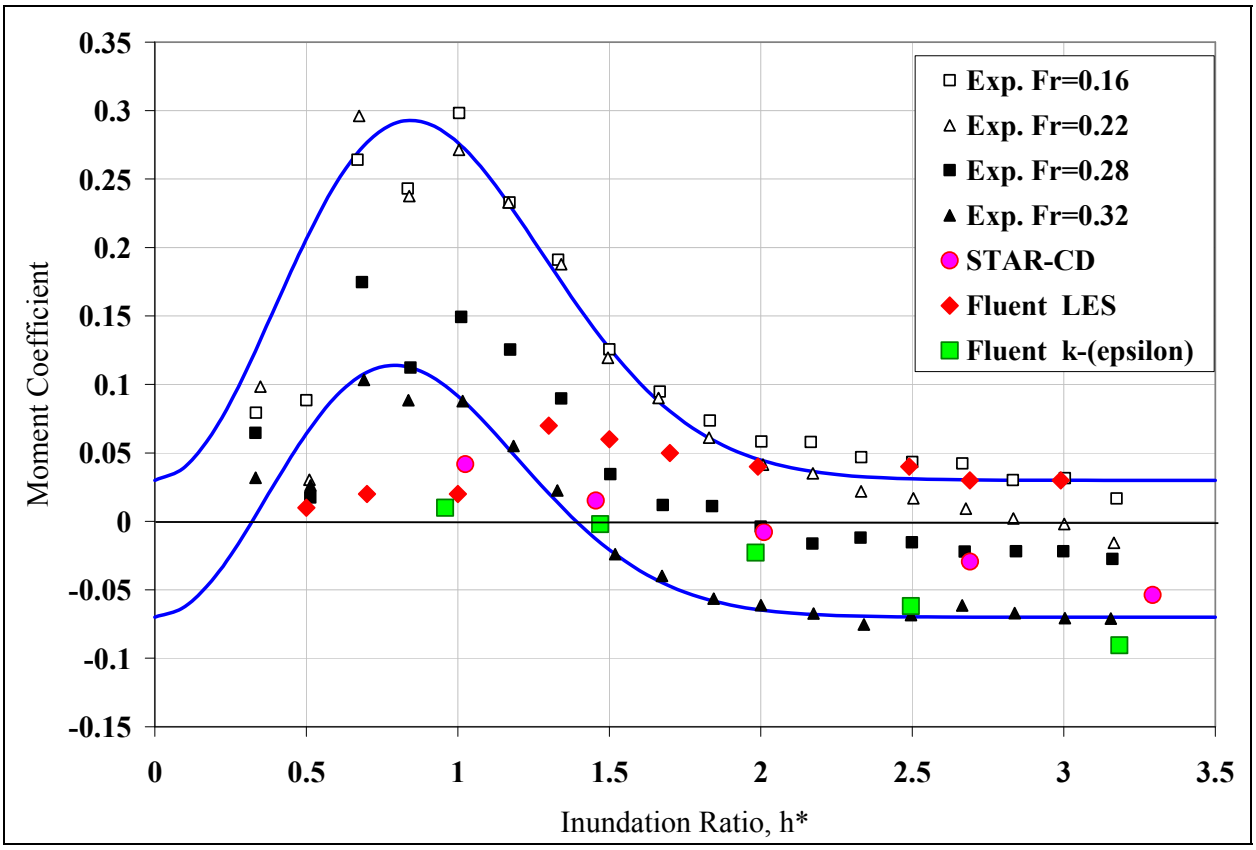


**Figure 30. Graph. Moment coefficient versus inundation ratio for the six-girder bridge.**

## RESULTS FOR THE THREE-GIRDER BRIDGE DECK

The three-girder bridge deck represented another common highway bridge design. The bridge-deck height was somewhat larger than the height for the six-girder, and the girders were rectangular and proportionally more massive. The increased deck height meant that the bridge could be tested for a narrower range of inundation ratios since the water depth remained at 0.25 m for all of the laboratory experiments.

Figure 31 shows the drag coefficient plot for the three-girder bridge. The experimental results display a shape similar to the results of the six-girder bridge, and the minimum point occurs at

roughly the same inundation ratio. The two higher *Fr* cases (0.28 and 0.32) tend to group fairly closely, as do the two lower *Fr* cases (0.16 and 0.22). Additionally, the drag coefficient stabilizes at a higher value for *Fr* = 0.28 than for *Fr* = 0.32.

The CFD results for the three-girder bridge are also displayed on the plot in figure 31. Unlike the simulations for the six-girder bridge, the flow conditions in the CFD model are not calibrated based on the experimental results. Instead, the configuration of the six-girder model is used, and only the bridge deck model is changed. The STAR-CD® model results show only a slight response to *Fr.* The results, as plotted, seems to agree most closely with the higher *Fr* experimental results. The Fluent® results for the unsteady, 3-D k-ε model display a general agreement with experimental results at lower *h** values but somewhat overestimate the drag coefficient at higher values.

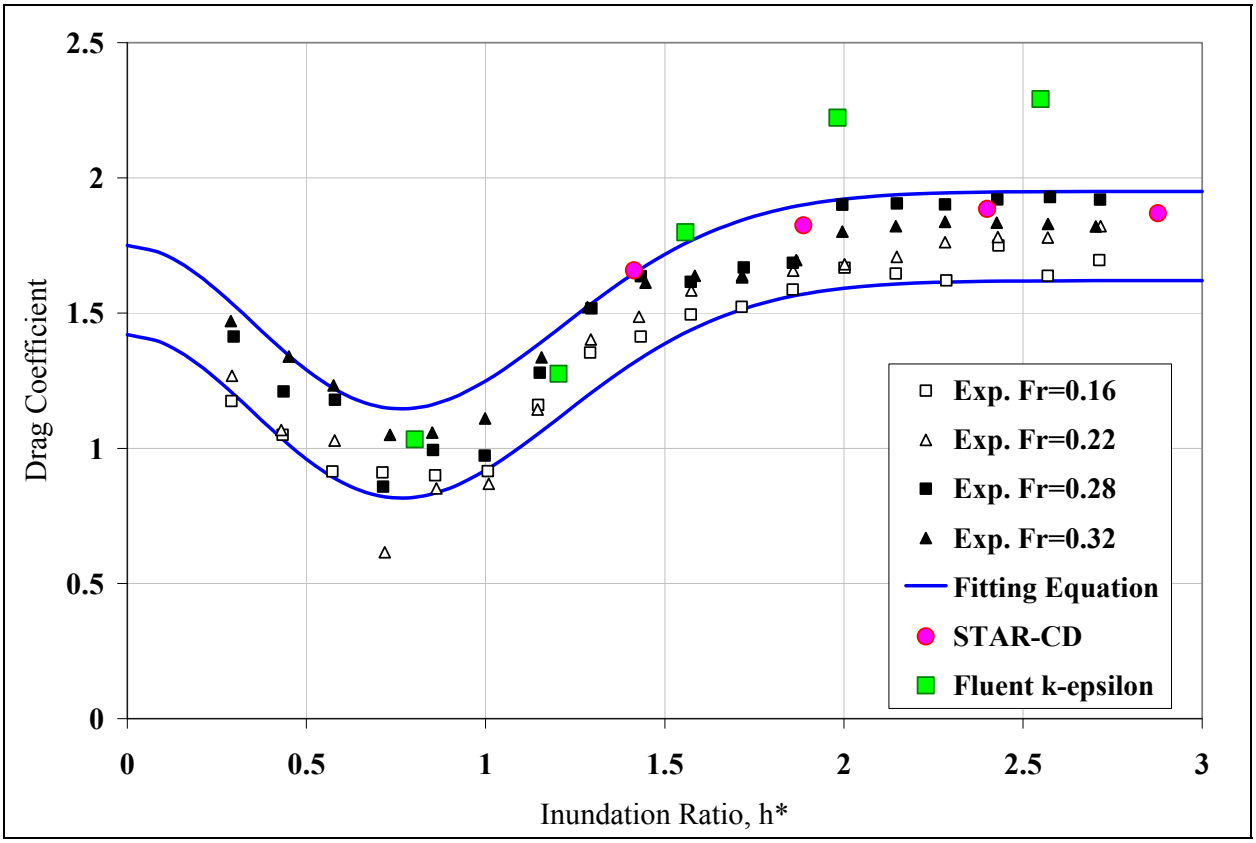


**Figure 31. Graph. Drag coefficient versus inundation ratio for the three-girder bridge.**

The lift coefficient plot in figure 32 shows a generally similar pattern to figure 29. The critical lift coefficient is slightly larger (more negative) for the three-girder deck. The three-girder deck shows a slightly more regular response to *Fr* as the experimental results do not cross each other nearly as much as in the six-girder experiments. The CFD results for both models replicate the lift forces fairly well, but the simulations do not capture the critical lift values.

The moment coefficient plot (figure 33) shows a similar shape to the moment plot for the six-girder bridge. The maximum positive moment occurs at an inundation ratio of approximately 0.8. The maximum moment coefficient value shown in the fitting is approximately 0.24, a reduction

from the 0.30 coefficient for the six-girder bridge. This difference may be partially explained by the first girder being set back further from the leading edge of the bridge deck. At high inundation ratios, the direction of the moment reverses and attains a maximum value of negative 0.11 according to the fitting equations. Neither of the CFD models seems to capture the positive moment coefficients. The STAR-CD® model fits the experimental data reasonably well at high inundation ratios, but the Fluent® k-ε model shows only weak agreement and a different shape.

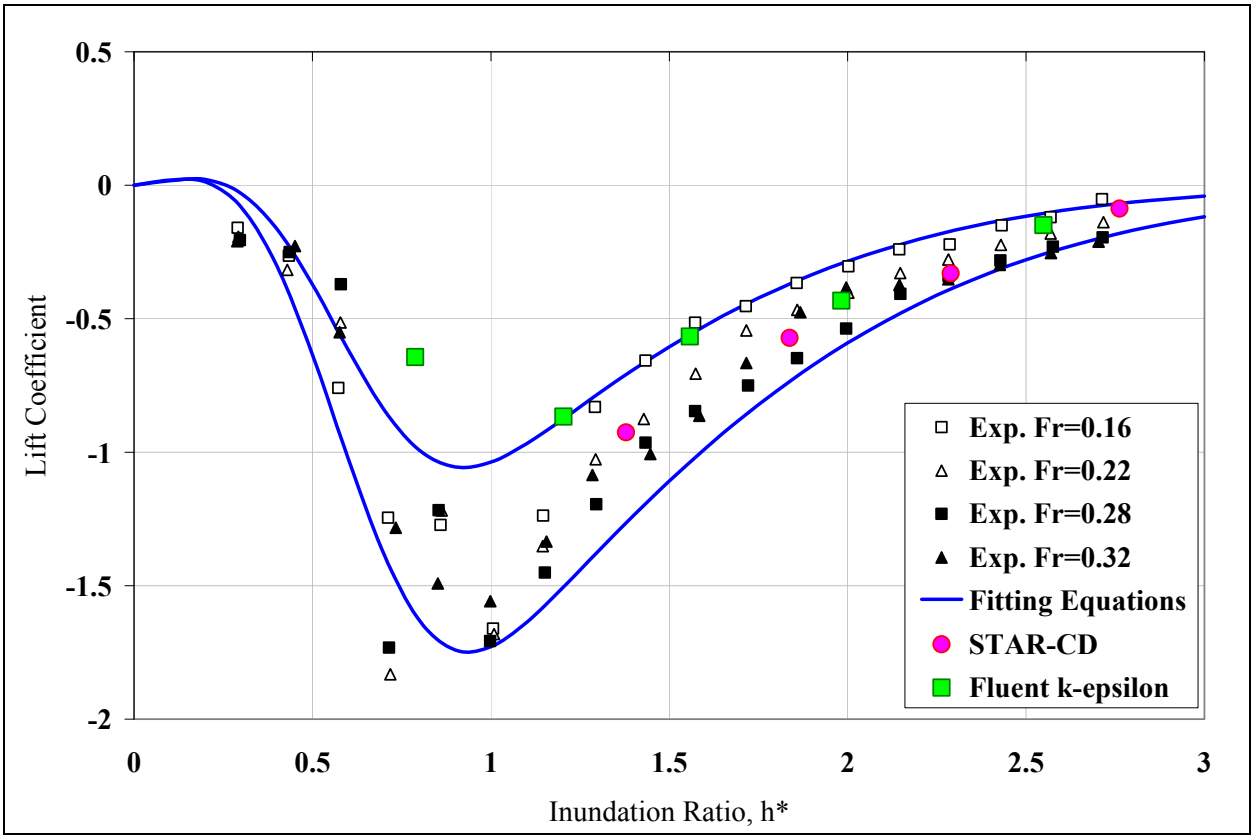


**Figure 32. Graph. Lift coefficient versus inundation ratio for the three-girder bridge.**

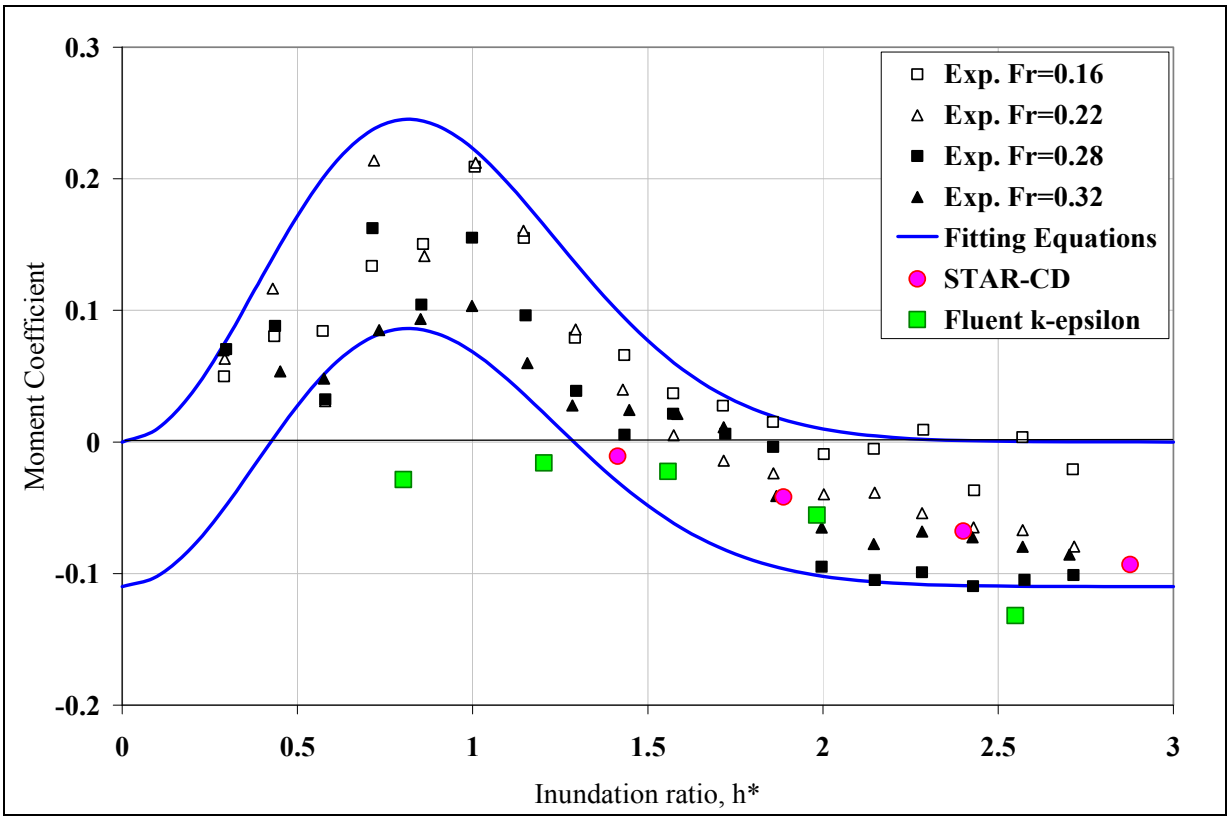


**Figure 33. Graph. Moment coefficient versus inundation ratio for three-girder bridge.**

## RESULTS FOR THE STREAMLINED DECK

This section presents the results for the streamlined bridge deck. Only one CFD model, a Fluent® k-ε model, was created for the streamlined bridge deck. As was the case with the three-girder deck, the flow configuration settings of the six-girder model were used for the streamlined deck because modeling results were not available for calibration.

Figure 34 shows the drag coefficient plot for the streamlined bridge deck. In contrast to the three- and six-girder bridge decks, the drag coefficients are significantly lower for the streamlined decks by a factor of roughly 50 percent. Additionally, the streamlined deck appears much less influenced by *Fr,* as all four sets of experimental results are tightly bunched. The experimental results have difficulty capturing data between 0.5 and 1 due to the model bridge deck's small profile. Nonetheless, the minimum drag coefficient value appears to occur at an inundation ratio of 1.2 versus roughly 0.8 for the other deck shapes.

The CFD results match the experimental results fairly well for the drag coefficient only. The CFD results for the lift and moment coefficient, however, do not match very well probably because the flow conditions were calibrated for the larger and differently shaped six-girder deck.

Figure 35 displays the lift coefficient plot. The data take a similar shape to the results for the other bridges. The critical value of roughly -1.2 represent a 20 to 25 percent reduction in pull-down force compared to the other two bridge shapes. The experimental results' variation by *Fr* is

dramatic, as there appears to be a strong grouping among the *Fr* = 0.22, 0.28, and 0.32 scenarios but then a wide gap to the *Fr* = 0.16 scenario.

The streamlined bridge's moment coefficient plot (figure 36) exhibits different behavior than the other moment plots. Notably, the shape of the experimental results does not follow a smooth curve up to a peak and then a smooth decline but rather abruptly go to a peak. The peak location is not known precisely due to a lack of data at $h^* < 1$, but the peak seems to occur at about $h^* = 1$ or less, which is interesting because the critical points of the lift and drag plots occur at somewhat higher values of $h^*$. The down slope of the experimental values also appears as two fairly linear segments (with a change to a flatter slope at roughly $h^* = 2.25$), rather than the smooth curve exhibited by the six-girder data. Overall, though, it is evident that the peak moment coefficient on the upper envelope curve of roughly 0.2 is about a 33 percent reduction from the six-girder coefficient.

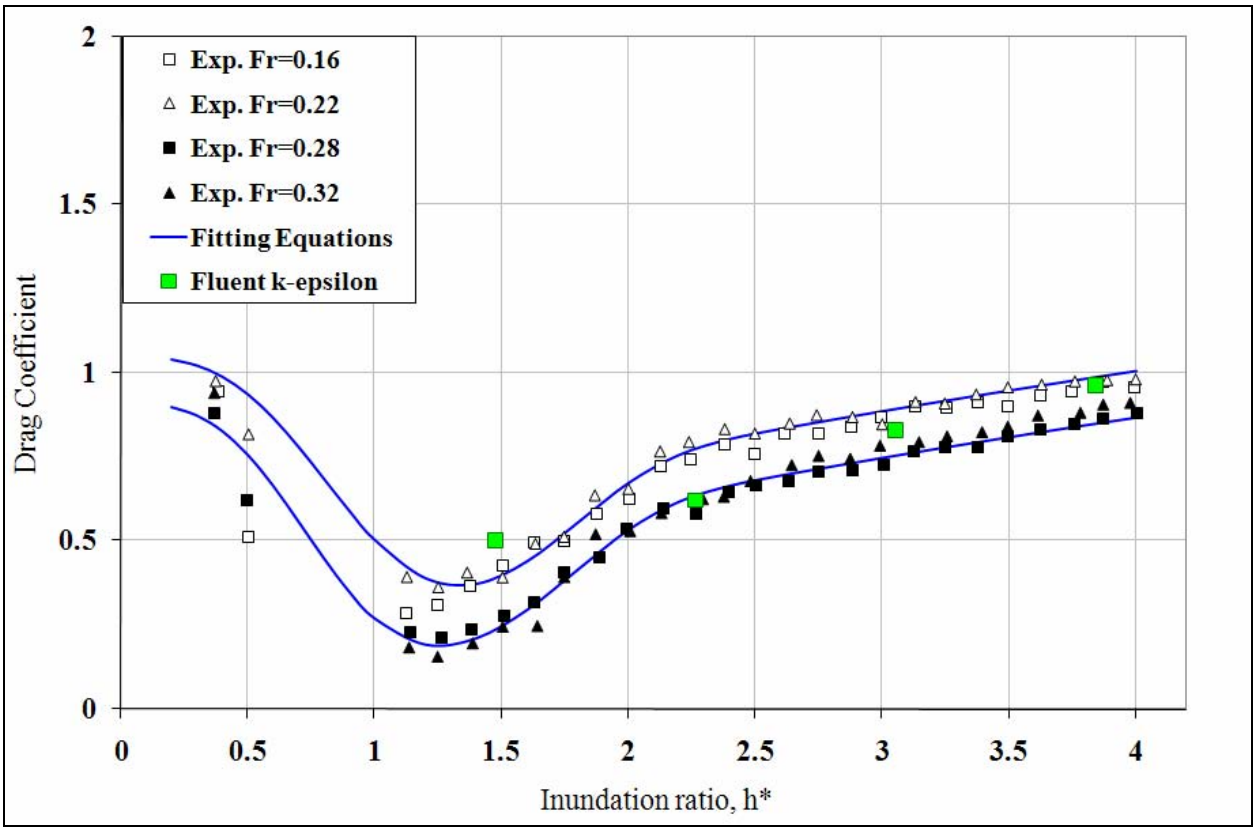


**Figure 34. Graph. Drag coefficient versus inundation ratio for streamlined bridge deck.**

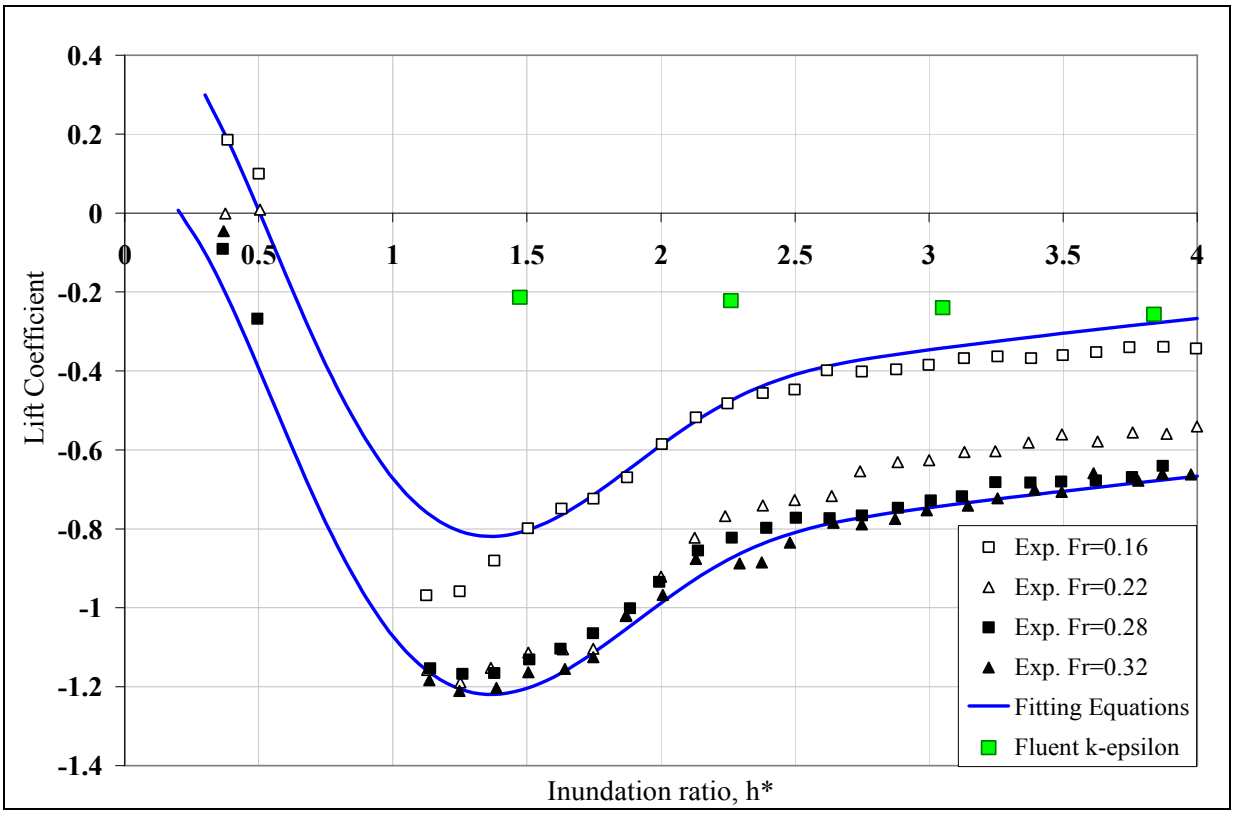


**Figure 35. Graph. Lift coefficient versus inundation ratio for the streamlined bridge.**

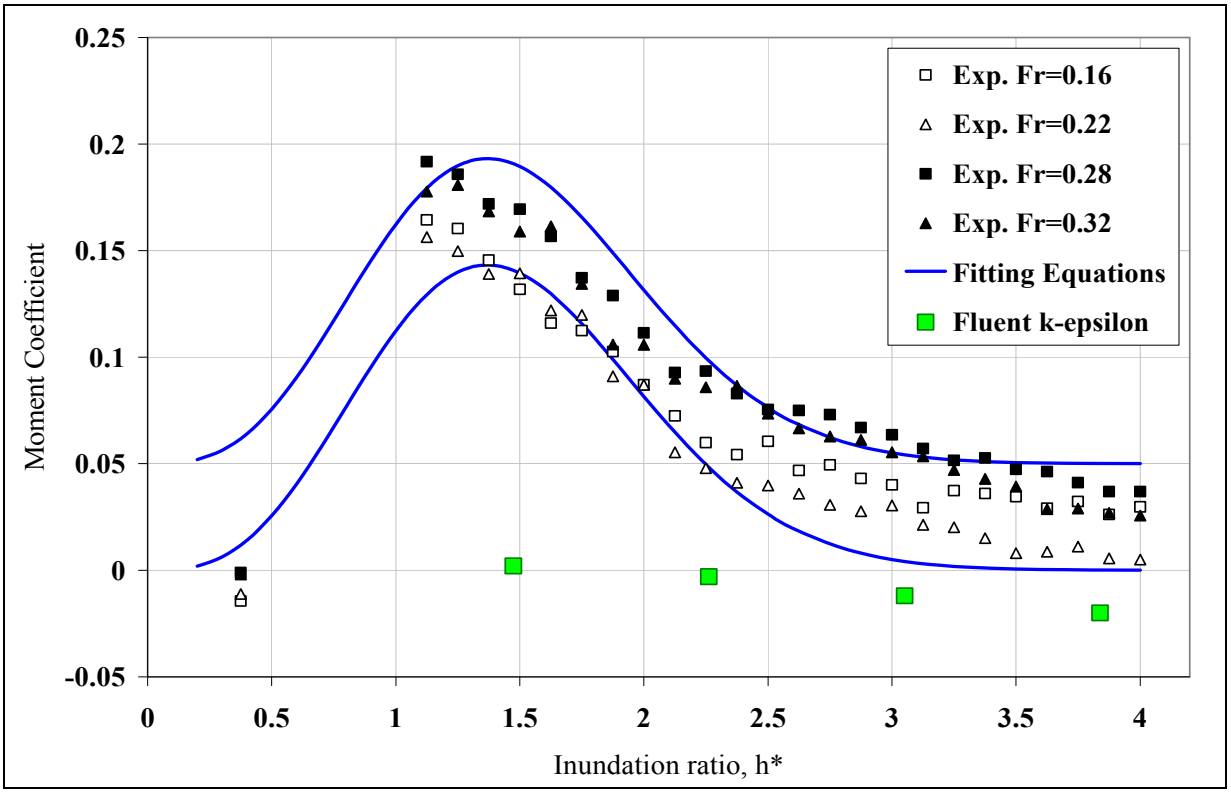


**Figure 36. Graph. Moment coefficient versus inundation ratio for the streamlined bridge.**

## FITTING EQUATIONS AND COEFFICIENT VALUES

This section provides the fitting equations for the curves shown on the plots and the necessary coefficient values to generate each fitting curve. The equation for each force or moment coefficient is given as a function of *h**. The upper and lower fitting curves for each individual plot always have the same equation form but have different coefficients. The fitting equations for the six-girder and three-girder bridge decks are of the same form and only need different coefficient values to describe their differences. The streamlined deck has a similar equation form to the other two bridge types for the moment equation but has a very different form for the drag and lift coefficient equations. Figure 37 to figure 41 show the forms of the fitting equations for the various bridges.

$$C_D = A \cdot e^{-2\cdot(h^*)^2} - B \cdot e^{-0.75\cdot(h^*)^2} + a$$

**Figure 37. Equation. Drag coefficient fitting equation for three- and six-girder bridges.**

$$C_L = b \cdot \left( e^{-3.5\cdot(h^*)^2} - e^{-c\cdot(h^*)^{1.7}} \right)$$

**Figure 38. Equation. Lift coefficient fitting equation for three- and six-girder bridges.**

$$C_M = d \cdot (h^*)^{\alpha} \cdot e^{-f\cdot(h^*)^2} + g$$

**Figure 39. Equation. Moment coefficient fitting equation for all bridge types.**

$$C_D = 0.8 \cdot e^{-m\cdot(h^*)^3} + 0.33 \cdot (h^*)^{0.6} \cdot \left( 1 - e^{-0.04\cdot(h^*)^{5.55}} \right) + n$$

**Figure 40. Equation. Drag coefficient fitting equation for the streamlined bridge.**

$$C_L = 1.5 \cdot e^{-1.6\cdot(h^*)^2} + 0.4213 \cdot (h^*)^{0.4} \left( 1 - e^{-0.0626\cdot(h^*)^{4.4147}} \right) - j$$

**Figure 41. Equation. Lift coefficient fitting equation for the streamlined bridge.**

The coefficients in the fitting equations (*A, B, a,* etc.) are given in table 1 for the six- and three-girder bridges and in table 2 for the streamlined bridge. With these coefficient values inserted into the proper equation, the envelope of force coefficients can be calculated for any desired value of *h**. The coefficient values allow the fitting equations to provide the high and low estimates of the force coefficient for each bridge type. In many cases, however, the designer needs only a single critical value of drag, lift, or moment to design the bridge.

To estimate the critical values, the designer can simply look at the design charts for a reasonable guess. Table 3 lists the critical force coefficient values as calculated by the fitting equations and the associated value of *h** ($h^*_{crit}$). The drag coefficient is critical at its maximum positive value. The fitting equations give one maximum at $h^* = 0$, but, in reality, drag is highest when *h** is roughly greater than 2.5 or 3. The fitting equation for drag for the streamlined deck increases steadily as *h** increases, but, since *h** would rarely exceed 5, the drag coefficient value at $h^* = 5$, is reported ($C_D = 1.1$). As in the physical experimentation results, the lift coefficient reaches its

critical value at its most negative. Unlike the drag coefficient, the critical $C_L$ value occurs near the transition from the partially inundated to completely inundated case (i.e., $h^*$ is close to 1).

**Table 1. Fitting equation coefficient values for six-girder (6-g) and three-girder (3-g) bridges.**

| Equation | A | B | a | b | c | d | f | g | α |
|---|---|---|---|---|---|---|---|---|---|
| 6-g upper | 2.7 | 2.7 | 2.15 | 2 | 0.65 | 1 | 1.4 | 0.03 | 2 |
| 6-g lower | 2.7 | 2.7 | 1.75 | 3 | 0.62 | 0.8 | 1.6 | -0.07 | 2 |
| 3-g upper | 1.8 | 2 | 1.95 | 2 | 0.6 | 1 | 1.5 | 0 | 2 |
| 3-g lower | 1.8 | 2 | 1.62 | 3 | 0.5 | 0.8 | 1.5 | -0.11 | 2 |

**Table 2. Fitting equation coefficient values for the streamlined bridge.**

| Equation | m | n | j | d | f | g | α |
|---|---|---|---|---|---|---|---|
| Streamlined upper | 1.2 | 0.25 | 1.4 | 0.25 | 0.8 | 0.05 | 3 |
| Streamlined lower | 1.7 | 0.11 | 1.0 | 0.25 | 0.8 | 0 | 3 |

**Table 3. Critical coefficient values by bridge type.**

| Bridge type | $C_D$ | $h^*_{crit}$ | $C_L$ | $h^*_{crit}$ | $C_M$ | $h^*_{crit}$ |
|---|---|---|---|---|---|---|
| 6-g | 2.15 | 0, > 3 | -1.644 | 0.8025 | 0.2927 hi<br>-0.07 lo | 0.8452<br>0, > 2.5 |
| 3-g | 1.95 | 0, > 3 | -1.815 | 0.8312 | 0.2453 hi<br>-0.11 lo | 0.8165<br>0, > 2.5 |
| Streamlined | ~ 1.1 | ~ 4 | -1.219 | 1.367 | 0.1932 | 1.369 |

## 5. DECK FORCE CALCULATION EXAMPLES

This section describes how to use the results of this study to estimate the force and moment coefficients on a proposed bridge design.

To calculate the force coefficient, the dimensions and elevation of the proposed bridge, the dimensions of the channel, and the velocity and inundation elevation of the stream at the flood of interest must be known.

Suppose a small six-girder bridge is planned with dimensions as in table 4.

**Table 4. Bridge example dimensions.**

| Dimension | Value |
|---|---|
| Deck thickness ($s$) | 2.5 m |
| Length ($L$) | 280 m |
| Width ($W$) | 11.2 m |
| Low chord elevation | 106 m (NAVD88) |

The bridge is planned over a small stream with an enormous range of flow. Suppose that the stream has a channel bottom elevation of 102 m at the crossing. The 50-year flood rises to an elevation of 105.9 m and is passed by the bridge. The 100-year flood has an elevation of 107.5 m and has an average stream velocity of 2.3 m/s. The 1,000-year flood rises to elevation 110 m and has an average velocity of 3.2 m/s.

Using these dimensions, $h_u$, $h_d$, $h^*$, and $Fr$ can be calculated. Table 5 calculates these flow conditions for the two floods.

**Table 5. Flow conditions for example design floods.**

| 100-year flood | 1,000-year flood |
|---|---|
| $h_u = 107.5 - 102 = 5.5$ m | $h_u = 10$ m |
| $h_b = 106 - 102 = 4$ m | $h_b = 4$ m |
| $h^* = (h_u - h_d)/s = (5.5 - 4)/2.5 = 0.6$ | $h^* = 2.4$ |
| $Fr = 2.3/(9.8 \times 5.5)^{0.5} = 0.313$ | $Fr = 0.323$ |

Supposing the bridge is a six-girder bridge deck, the force coefficients can be calculated for the two floods using the equations in figure 37 to figure 39 and the appropriate coefficients in table 3.

For example, to compute the drag coefficient for the 100-year flood, take the equation in figure 37 and apply the six-girder, high estimate coefficients to get $C_D$ as a function of $h^*$ as in figure 42.

$$C_D(h^*) = 2.7e^{-2\cdot(h^*)^2} - 2.7e^{-0.75\cdot(h^*)^2} + 2.15$$

**Figure 42. Equation. Upper fitting equation for drag coefficient as a function of *h**.**

For the 100-year flood, substitute $h^* = 0.6$ into the 6-g upper equation (figure 42) to find the high estimate of $C_D$ equals 1.403. A similar process is followed to get the force coefficient values in table 6 for both example floods.

**Table 6. High and low force coefficients for the two example floods.**

| Force coefficient | 100-year high | 100-year low | 1,000-year high | 1,000-year low |
|---|---|---|---|---|
| $C_D$ | 1.403 | 1.003 | 2.114 | 1.714 |
| $C_L$ | -0.955 | -1.462 | -0.112 | -0.192 |
| $C_M$ | 0.247 | 0.092 | 0.0318 | -0.0695 |

Table 6 shows that the 1,000-year flood has the higher force coefficient when the drag force is considered, but, for the lift force and moment, the 100-year flood values are more important. It should be noted that the $h^*_{crit}$ value occurs between the two floods for the lift and moment coefficients, so for design purposes, it is preferable to use the critical coefficient values in table 3.

Figure 5 through figure 7 allow the total forces and moments to be calculated. For instance, figure 5 can be rewritten to express the total drag force per unit length, as shown in figure 43, which inserts the bridge dimensions and flow values for the 1,000-year flood and solves the force as approximately 27.1 kilonewtons per meter (kN/m).

$$\frac{F_D}{L} = C_D \frac{1}{2}\rho v^2 s = 2.114\frac{1}{2}\cdot 3.2^2 \cdot 2.5 = 27{,}100 \quad N/m$$

**Figure 43. Equation. Total drag force per unit length on the example six-girder bridge for the 1,000-year flood.**

The designer may calculate the maximum drag force by knowing the velocity at the critical value of $h^*$, which can be computed if the $Fr$ is assumed to be constant. By combining figure 2 and figure 3 and keeping the $Fr$ constant, velocity equals 3.43 m/s (at $h^* = 3$), as shown in figure 44.

$$\mathbf{v} = \mathbf{Fr}\sqrt{\mathbf{g}\cdot\left(\mathbf{h^*_{crit}}\cdot\mathbf{s}+\mathbf{h_b}\right)} = 0.323\cdot\sqrt{9.8\cdot\left(3\cdot 2.5+4\right)} = 3.43\,\mathrm{m/s}$$

**Figure 44. Equation. Velocity, *v,* at $h^*_{crit}$.**

Using the velocity from figure 44 and the critical value of $C_D$ (2.15), the total drag force is 31.6 kN/m. Now, suppose a streamlined bridge is considered instead of the six-girder bridge. While *L, W,* and $h_b$ remain the same, the bridge thickness is reduced by the same proportion as the experimental prototypes to $s$ = 1.64 m. The critical value of $C_D$ for the streamlined bridge is 1.1 at roughly $h^*$ = 5, or 4.57 if the velocity remains the same. Solving the equation in figure 43 with the streamlined parameters, the total drag force is 11.2 kN/m, which is a sizeable reduction from the six-girder bridge. Similar calculations may be followed to analyze the lift force and moment.

# 6. CONCLUSION

Understanding the forces acting on inundated bridge decks is a worthwhile pursuit to improve the durability of bridges which can, even if infrequently, be overtopped in flooding events. The study described in this report investigated the properties of three common bridge deck types by measuring the response of drag force, lift force, and overturning moment to changes in the inundation ratio.

Experiments on scale models of the three bridge deck types were performed with an ultra-precise force balance. These experiments defined the general response of the force coefficients to different flow conditions, inundation ratios, and bridge types. The following key conclusions can be made about the forces on bridge decks from the experiments:

- The drag, lift, and moment coefficients showed a definite response to the inundation ratio, especially near the partially inundated to completely inundated transition ($h^* = 1$). The lift and moment coefficients increased in overall magnitude and reached their critical values in this zone. The drag coefficient, however, was reduced in overall magnitude in this transition zone and reached a stable critical value as the inundation ratio increased.

- The *Fr* had an influence on the force and moment coefficients. The *Fr* did not greatly influence the shape of the response to the inundation ratio but instead acted as a roughly constant offset. The total variation between the highest and lowest *Fr* (or the upper and lower fitting equations) depended on the type of bridge. The streamlined bridge had a much smaller envelope of coefficient values than the six- or three-girder bridges.

- The bridge type had an influence on the coefficient values. The six-girder bridge had the highest critical values for the drag and moment coefficients while the three-girder had the most critical lift coefficient. In general, the streamlined bridge deck showed a reduction in all three force coefficients under the same flow conditions as the other bridge types.

Overall, the experimental results provide the bridge designer with a wealth of information on the bridges' response to hydrodynamic forces when inundated. The design charts, fitting equations, and critical coefficient values provide a great deal of useful information for designing more durable bridges. In the future, however, more research will be needed to investigate the forces on the bridge deck in the region of transition from the partially inundated to completely inundated case as the critical lift (or pull-down) and moment values occur in this region.

CFD modeling was also performed as an alternative method to estimate the forces acting on bridge decks. Two CFD software packages, STAR-CD® and Fluent®, were used to model the bridge deck. A wide range of simulation options were explored, and the models reproduced the flow conditions of the experiments reasonably well, as judged by velocity map comparisons with the PIV results.

The CFD models performed reasonably well at estimating the force coefficient for the six-girder bridge for certain ranges of inundation coefficients. The models performed fairly poorly in reproducing the critical coefficient values and, in some cases, failed to match the behavior of the coefficients' response to $h^*$ in general. The three-girder and streamlined bridge CFD results did

not match the experimental values because they were calibrated using flow conditions from the six-girder experiments. Recalibrating the flow conditions for these models could lead to substantial improvements.

The CFD modeling showed great promise for estimating the performance of inundated bridge decks. While the models did not capture the full range of behavior shown in the experimental results, the estimates of forces showed enough similarity that further refinements may make the CFD models capable of producing a reliable projection of force coefficients for design purposes. The flexibility of CFD models to represent almost any scenario means that they have a definite upside over physical experimentation.

HRDI-07/05-09(WEB)E